Article

Developmental Cell

Repurposing of the multiciliation gene regulatory network in fate specification of Cajal-Retzius neurons

Graphical abstract

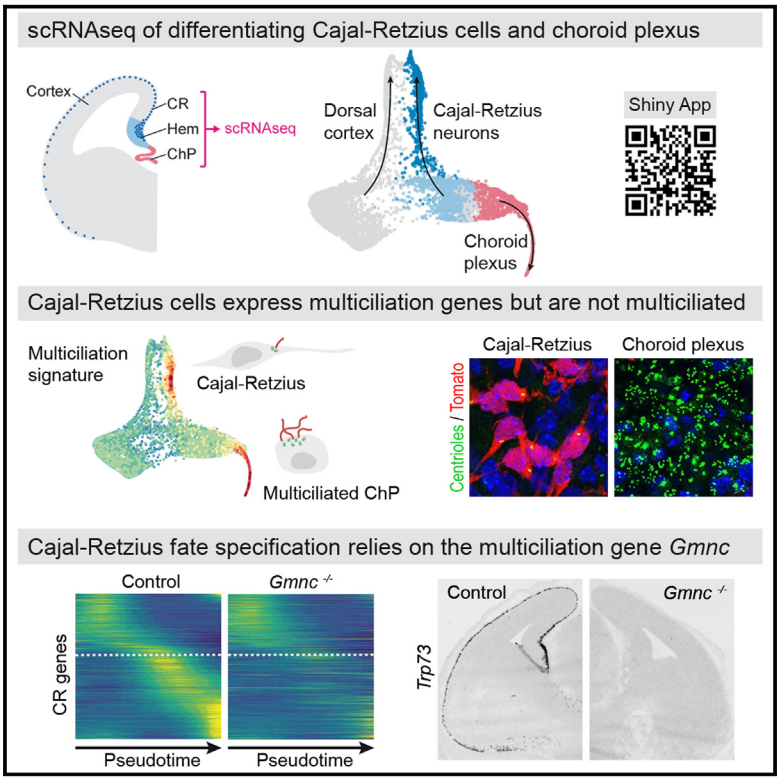

Highlights

- Differentiating Cajal-Retzius cells transiently express multiciliation genes
- Cajal-Retzius cells are not multiciliated
- Cajal-Retzius cell fate specification relies on the multiciliation master gene *Gmnc*
- *Trp73* lies downstream *Gmnc* during Cajal-Retzius cells fate specification

Authors

Matthieu X. Moreau, Yoann Saillour, Vicente Elorriaga, ..., Nathalie Spassky, Alessandra Pierani, Frédéric Causeret

Correspondence

frederic.causeret@inserm.fr

In brief

Moreau et al. investigate the mechanisms that control fate specification of Cajal-Retzius cells, a transient neuronal type that is essential for cerebral cortex development. They demonstrate that the gene regulatory network involved in multiciliogenesis was co-opted and repurposed in Cajal-Retzius cells, illustrating how novel cell identities may emerge.

Moreau et al., 2023, Developmental Cell *58*, 1–18
August 7, 2023
https://doi.org/10.1016/j.devcel.2023.05.011

CellPress

Please cite this article in press as: Moreau et al., Repurposing of the multiciliation gene regulatory network in fate specification of Cajal-Retzius neurons, Developmental Cell (2023), https://doi.org/10.1016/j.devcel.2023.05.011

Developmental Cell

CellPress

Article

Repurposing of the multiciliation gene regulatory network in fate specification of Cajal-Retzius neurons

Matthieu X. Moreau,[1,2] Yoann Saillour,[1,2] Vicente Elorriaga,[1,2] Benoît Bouloudi,[3] Elodie Delberghe,[1,2] Tanya Deutsch Guerrero,[1,2] Amaia Ochandorena-Saa,[4] Laura Maeso-Alonso,[5] Margarita M. Marques,[6] Maria C. Marin,[5] Nathalie Spassky,[3] Alessandra Pierani,[1,2] and Frédéric Causeret[1,2,7,*]

[1]Université Paris Cité, *Imagine* Institute, Team Genetics and Development of the Cerebral Cortex, 75015 Paris, France
[2]Université Paris Cité, Institute of Psychiatry and Neuroscience of Paris, INSERM U1266, 75014 Paris, France
[3]Institut de Biologie de l'Ecole Normale Supérieure (IBENS), Département de Biologie, Ecole Normale Supérieure, CNRS, INSERM, Université PSL, 75005 Paris, France
[4]Université Paris Cité, Imagine-Institut Pasteur, Unit of Heart Morphogenesis, INSERM UMR1163, 75015 Paris, France
[5]Instituto de Biomedicina, y Departamento de Biología Molecular, Universidad de León, 24071 Leon, Spain
[6]Instituto de Desarrollo Ganadero y Sanidad Animal, y Departamento de Producción Animal, Universidad de León, 24071 Leon, Spain
[7]Lead contact
*Correspondence: frederic.causeret@inserm.fr
https://doi.org/10.1016/j.devcel.2023.05.011

SUMMARY

Cajal-Retzius cells (CRs) are key players in cerebral cortex development, and they display a unique transcriptomic identity. Here, we use scRNA-seq to reconstruct the differentiation trajectory of mouse hem-derived CRs, and we unravel the transient expression of a complete gene module previously known to control multiciliogenesis. However, CRs do not undergo centriole amplification or multiciliation. Upon deletion of *Gmnc*, the master regulator of multiciliogenesis, CRs are initially produced but fail to reach their normal identity resulting in their massive apoptosis. We further dissect the contribution of multiciliation effector genes and identify *Trp73* as a key determinant. Finally, we use *in utero* electroporation to demonstrate that the intrinsic competence of hem progenitors as well as the heterochronic expression of *Gmnc* prevent centriole amplification in the CR lineage. Our work exemplifies how the co-option of a complete gene module, repurposed to control a distinct process, may contribute to the emergence of novel cell identities.

INTRODUCTION

Cajal-Retzius cells (CRs) are transient glutamatergic neurons of the developing forebrain that reside in the marginal zone (MZ) until their elimination by apoptosis during the first postnatal weeks in rodents.[1,2] Since their discovery more than a century ago by S. Ramon y Cajal and G. Retzius,[3,4] they have been shown to play a fundamental role in the control of cortical lamination,[5] arealization,[6,7] and circuit formation[8–12] via the secretion of signaling factors, including Reelin.[13,14] CRs presence is currently reported in amniotes only, and their abundance in the mammalian dorsal pallium (DP) led to propose they could have contributed to brain complexification during evolution.[15]

In mouse, CRs are generated between embryonic days (E) 10.5 and E13.5[16,17] in discrete pallial progenitors domains located at the border of the cortical primordium, from which they migrate tangentially in the MZ to cover the entire cortical surface. Genetic tracing experiments allowed the identification of four distinct origins for CRs, three of which are located in medial regions: the septum rostrally,[18] the cortical hem that produces most neocortical CRs,[16,19] and the thalamic eminence (ThE) caudally.[20,21] An additional described origin corresponds to the pallial-subpallial boundary (PSB), also referred to as ventral pallium.[18] We have previously shown that hem-, septum-, and ThE-derived CRs (subsequently referred to as medial CRs) share the expression of a highly specific gene module comprising *Trp73*, *Lhx1*, *Cdkn1a* (p21), *Ebf3*, and *Cacna2d2*, among other genes, distinguishing them from PSB-derived CRs that lack such signature.[22] However, all subtypes share common features: they are the only *Foxg1*-negative neurons in the developing cerebral cortex and additionally express high levels of *Reln* and *Nhlh2*.[22] In *Foxg1*-deficient mice, cortical neurons abnormally express Reln, suggesting that CRs represent the default fate unless repressed by Foxg1.[23] However, only *Trp73*$^{-}$ CRs are produced upon conditional inactivation of *Foxg1* at E13,[24] pointing to additional mechanisms involved in the specification of medial CRs. To date, such mechanisms remain completely elusive.

Interestingly, medial CR markers *Trp73* and *Cdkn1a* were recently involved in multiciliation,[25,26] the cellular process consisting in the amplification of centrioles followed by the growth of multiple motile cilia. The central nervous system of all

Please cite this article in press as: Moreau et al., Repurposing of the multiciliation gene regulatory network in fate specification of Cajal-Retzius neurons, Developmental Cell (2023), https://doi.org/10.1016/j.devcel.2023.05.011

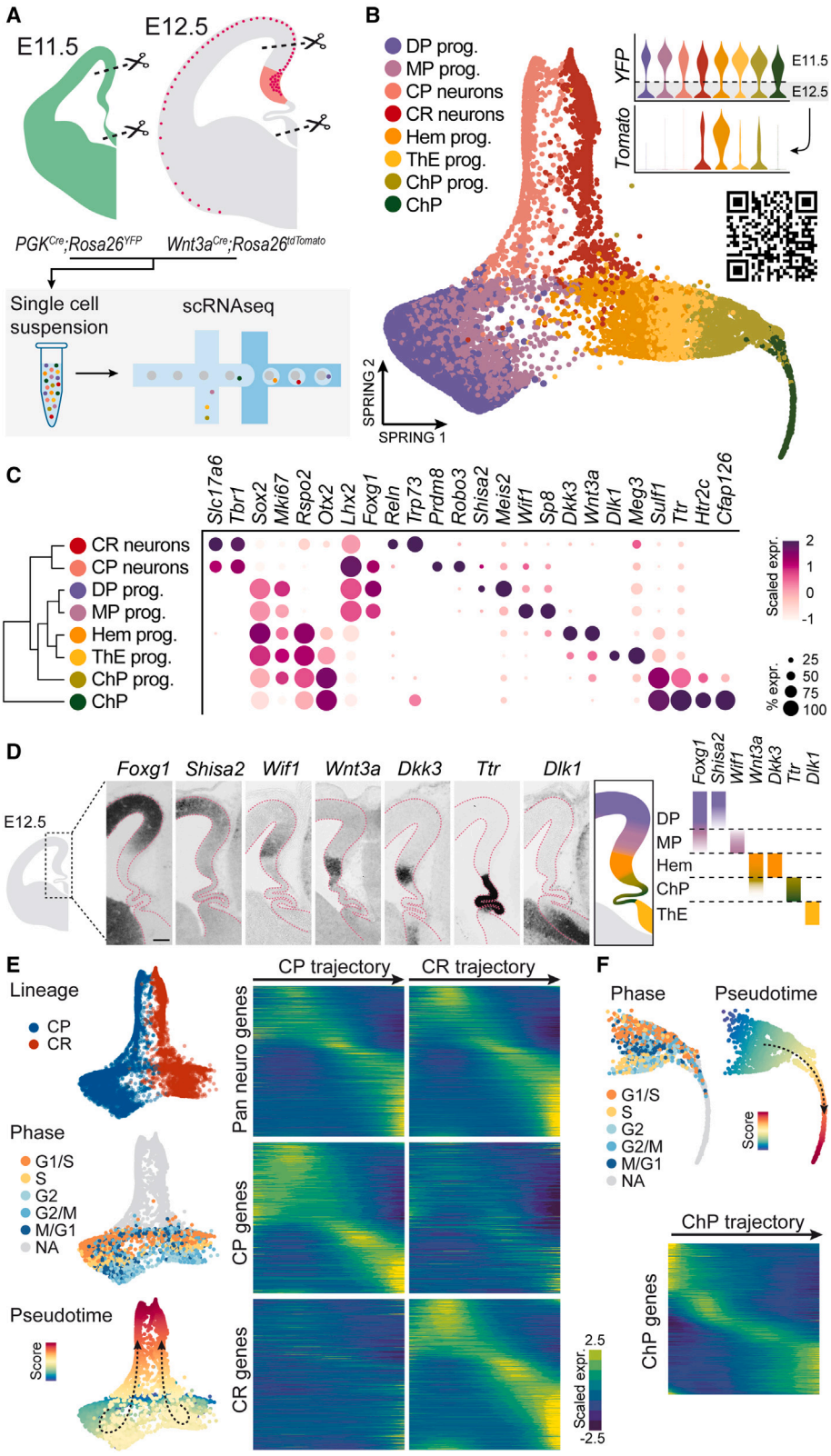

(legend on next page)

Please cite this article in press as: Moreau et al., Repurposing of the multiciliation gene regulatory network in fate specification of Cajal-Retzius neurons, Developmental Cell (2023), https://doi.org/10.1016/j.devcel.2023.05.011

vertebrates is lined by multiciliated ependymal cells, and multiciliated cells of the choroid plexus (ChP) secrete the cerebrospinal fluid.[27,28] The gene regulatory network controlling multiciliation is also highly conserved between organs and species. The chromatin regulator GemC1, encoded by *Gmnc*, is both necessary and sufficient for multiciliation and was shown to control the expression of most components of the multiciliation cascade, including *Trp73* and *Cdkn1a*.[25,29–31]

In this study, we used single-cell RNA sequencing (scRNA-seq) to investigate the mechanisms involved in the specification of medial CRs, focusing on the most abundant source located at the hem. We found that all components of the multiciliation gene regulatory network are expressed transiently at early steps of CR differentiation. However, CRs do not amplify their centrioles or grow multiple cilia. We disrupted the multiciliation regulatory network to demonstrate that *Gmnc* is required for CR specification. In its absence, CRs are produced, acquire some characteristic features (*Reln* expression and tangential migration), but fail to maintain their identity and undergo cell death. *Trp73* mutants completely phenocopy *Gmnc*-deficient animals, unlike *Ccdc67*/*Deup1*, *Ccno*, or *Ccdc40* mutants, pointing to a differential requirement of multiciliation genes in CRs specification. Using *in utero* electroporation, we demonstrate that competence of the hem territory as well as heterochrony in *Gmnc* expression restricts its ability to induce multiciliation. Our work exemplifies how a gene network can be co-opted and repurposed to perform a function completely distinct from its original one.

RESULTS

Transcriptomic characterization of the early medial telencephalon

In mouse, the cortical hem is the main source of neocortical CRs.[19] In order to better understand the process of CR specification, we performed scRNA-seq on dissected tissue encompassing the hem (Figure 1A). To ensure sufficient sampling of CR progenitors, precursors, and neurons, we pooled tissue obtained from six E11.5 and four E12.5 embryos. E11.5 samples were collected from $PGK^{Cre};Rosa26^{YFP}$ embryos and E12.5 cells were obtained from $Wnt3a^{Cre};Rosa26^{tdTomato}$ animals to enable the deconvolution of each stage on the basis of *YFP* sequencing reads, and the identification of E12.5 hem and hem-derived cells thanks to *Tomato* expression (Figures S1A–S1C).

After quality control and filtering, we obtained 15,160 cells with a median 3,750 genes detected per cell, which were subject to iterative clustering and annotation based on known marker genes. Projection of these cells on a low-dimensional SPRING embedding (Figure 1B) identified 5 clusters containing cycling progenitors, collectively identified by the expression of *Sox2* and *Mki67* (Figures 1B, 1C, and S1E). dorsal pallium (DP) and medial pallium (MP) progenitors, both $Foxg1^{+}/Lhx2^{high}$, were distinguished by the expressions of *Shisa2*/*Meis2* and *Wif1*/*Sp8*, respectively (Figures 1C and S1E). They segregated away from the hem, ThE, and ChP progenitors, all $Rspo2^{+}/Otx2^{+}$, and best identified by the expressions of *Dkk3*/*Wnt3a*, *Dlk1*/*Meg3*, and *Sulf1*/*Ttr*, respectively. Tissue mapping of these progenitor domains by *in situ* hybridization (ISH) highlighted their spatial segregation and confirmed the sharp distinction between the abutting MP and hem (Figures 1D, S1E, and S1F). Three post-mitotic differentiation trajectories emerged from those progenitors: two of them contained pallial glutamatergic neurons ($Tbr1^{+}/Slc17a6^{+}$) and corresponded to cortical plate (CP) neurons ($Prdm8^{+}/Robo3^{+}$) and CRs ($Trp73^{+}/Reln^{high}$), whereas the remaining one was identified as ChP ($Htr2c^{+}/Cfap126^{+}$). YFP^{+} cells (collected at E11.5) were found in all clusters with a contribution of ~65%, showing no strong cell composition bias between stages (Figures S1A and S1C). $Tomato^{+}$ cells (belonging to the Wnt3a lineage) were most abundant in the hem, CR, and ChP progenitors clusters (Figure 1B), consistent with Yoshida et al.[19] Of note, the few $Tomato^{+}$ cells found in the ThE cluster probably reflect imperfect clustering (likely caused by the transcriptional continuity between Hem and ThE progenitors) rather than the real presence of Wnt3a-derived cells in this tissue, consistent with previous reports (see Figure 3A of Ruiz-Reig et al.[20]).

We then reconstructed the transcriptional trajectory followed by CP neurons, CRs, and ChP throughout the specification and early differentiation steps. The parallel arrangement of the two neuronal trajectories suggest they share the sequential expression of pan-neuronal transcriptional modules and differ by sets of lineage-specific genes. CR and CP neurons, together with their progenitors of origin, were aligned along a pseudotime axis to extract such common or lineage-specific genes and characterize their expression dynamics during fate commitment and early differentiation (Figure 1E; Table S2). A similar strategy was used to characterize the transcriptional dynamics during ChP differentiation (Figure 1F; Table S3). Importantly, the high cellular sampling in each lineage allowed us to capture the successive transient cell states at relatively high resolution. The approach was validated by the observation that pan-neuronal genes such as *Sox2*, *Neurog2*, and *Tbr1* were sequentially expressed with similar dynamics in the two neuronal lineages, whereas *Wnt3a*, *Trp73*, and *Lhx1* or *Tgfb2*, *Rprm*, and *Prdm8* were specifically and sequentially expressed along CR and CP trajectories, respectively (Figure S1G).

We therefore generated a high-resolution transcriptomic atlas of the hem and surrounding regions of the early developing

Figure 1. Transcriptional landscape around the early mouse hem

(A) The hem region from six E11.5 $PGK^{Cre};Rosa26^{YFP}$ and four E12.5 $Wnt3a^{Cre};Rosa26^{tdTomato}$ mouse embryos was subjected to scRNA-seq.

(B) 2D representation of the dataset after SPRING dimensionality reduction. Violin plots depict the contribution of YFP^{+} and $Tomato^{+}$ cells. The QR code points to the Shiny App allowing to browse the data.

(C) Bubble plot showing differential gene expression between clusters.

(D) ISH on coronal sections of E12.5 forebrain for selected genes. Scale bar, 100 μm.

(E) Reconstruction of CRs and CP differentiation trajectories (left). Heatmaps (right) represent gene expression along pseudotime for each lineage, using genes common or specific to each trajectory.

(F) Reconstruction of ChP differentiation trajectory and identification of genes differentially expressed along pseudotime. DP, dorsal pallium; MP, medial pallium; CP, cortical plate; CR, Cajal-Retzius; ThE, thalamic eminence; ChP, choroid plexus. See also Figure S1 and Table S3.

Please cite this article in press as: Moreau et al., Repurposing of the multiciliation gene regulatory network in fate specification of Cajal-Retzius neurons, Developmental Cell (2023), https://doi.org/10.1016/j.devcel.2023.05.011

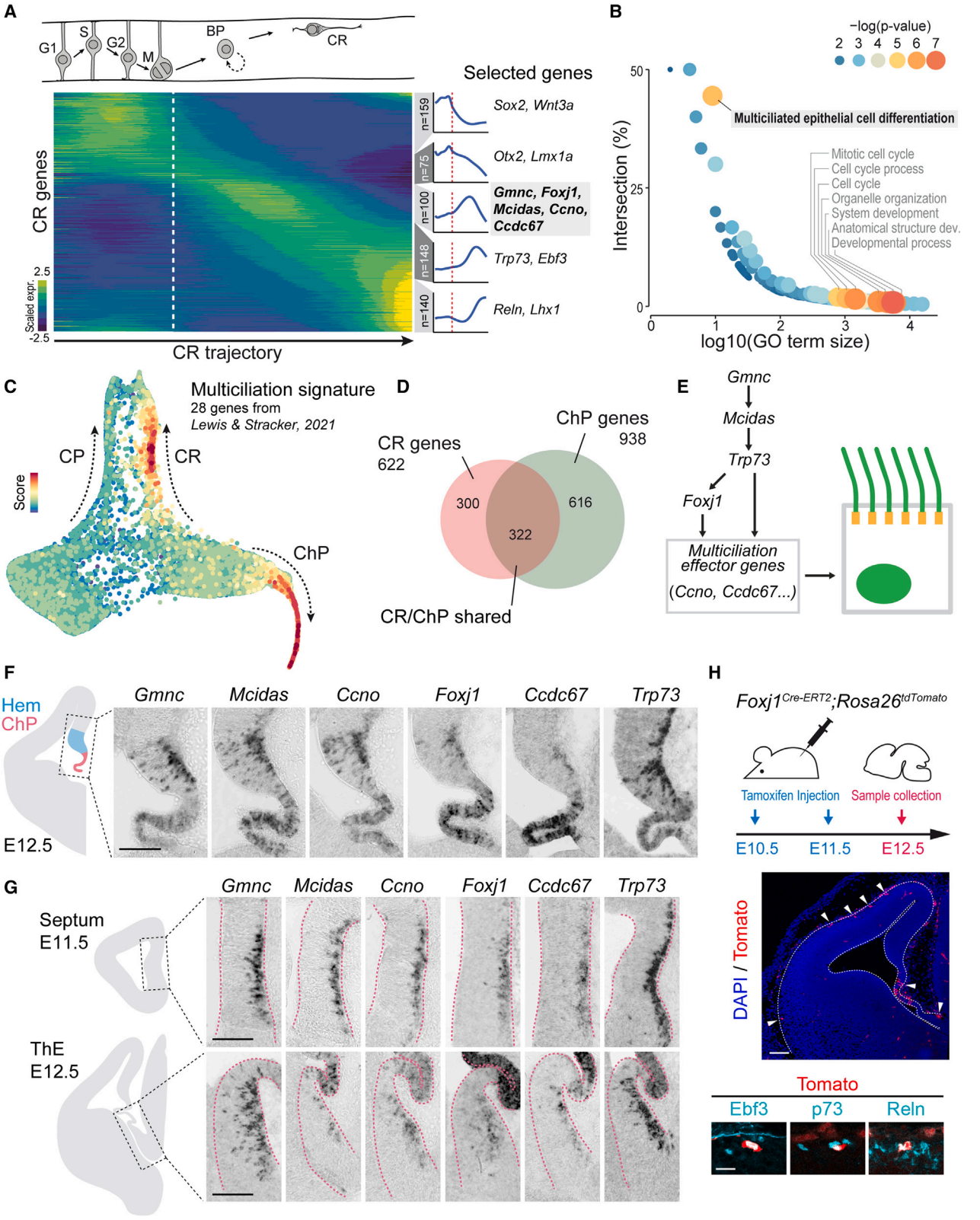

Figure 2. Expression of multiciliation genes in differentiating CR cells

(A) Heatmap depicting gene expression during CRs differentiation. The trends of the successive gene waves are shown on the right. Selected genes are indicated for each wave. Dashed lines mark the exit of apical progenitor state.

(legend continued on next page)

Please cite this article in press as: Moreau et al., Repurposing of the multiciliation gene regulatory network in fate specification of Cajal-Retzius neurons, Developmental Cell (2023), https://doi.org/10.1016/j.devcel.2023.05.011

telencephalon, including plain differentiation trajectories for CR, CP, and ChP lineages. We provide a web-based user-friendly Shiny App interface to visualize the data (available at https://apps.institutimagine.org/mouse_hem/).

CR cells transiently express multiciliation genes but are not multiciliated

Since mature CRs harbor a very peculiar transcriptomic signature compared with other cortical excitatory neurons,[1,22,32] we speculated that they should express lineage-specific fate determinants at the onset of their differentiation. We therefore focused on the 100 genes upregulated upon commitment to neuronal differentiation in the CR lineage but not in CP neurons (Figure 2A; Table S2). In order to identify pathways possibly involved in CR fate specification, we subjected these genes to a gene ontology (GO) enrichment analysis that surprisingly indicated a significant over-representation of genes associated with the differentiation of multiciliated cells (Figure 2B). We therefore computed a multiciliation signature, consisting of 28 genes currently known to regulate this process,[33] to find out that their expression during CR differentiation is transiently upregulated at levels matching that of ChP (Figure 2C). By contrast, CP neurons displayed low expression of the multiciliation gene module throughout differentiation. We then wondered what could be the extent of transcriptomic similarity between differentiating CRs and ChP. We found that among the 622 genes specific to the CR trajectory, more than half (322) were shared with ChP (Figure 2D; Table S4). This indicates a major overlap between the differentiation programs at play in both cell types, extending well beyond the few dozens of known multiciliation genes. Nevertheless, CRs and ChP each displayed strong specific signatures, consistent with their distinct specialization.

At the individual gene level, we found that the main components of the multiciliation network (Figure 2E) exhibit distinct expression dynamics, with the master regulator *Gmnc* starting at the exit of apical progenitor state and preceding all other genes, as exemplified with *Mcidas*, *Ccno*, *Foxj1*, *Ccdc67/Deup1*, and *Trp73* (Figures S2A and S2B). ISH experiments indicated overlapping expression of these genes in the hem (Figure 2F), septum, and ThE (Figure 2G), contrasting with the PSB where we never detected expression (not illustrated). All multiciliation genes, to the exception of *Trp73*, were expressed transiently in differentiating CRs, showing a strong downregulation when they engage tangential migration in the neocortex. The additional analysis of two scRNA-seq atlases of the developing cerebral cortex published by La Manno et al.[34] and Di Bella et al.[35] yielded similar results (Figures S2C and S2D).

To formally confirm those findings, we crossed the *Foxj1*$^{Cre\text{-}ERT2}$ mouse line with the *Rosa26*^{tdTomato} reporter strain and performed tamoxifen injections at E10.5 and E11.5 to permanently label the early-born progeny of *Foxj1*-expressing cells. Embryos collected at E12.5 showed numerous Tomato$^+$ cells occupying the characteristic superficial position of CRs in the developing cortex and immunoreactive for CR markers (either Ebf3, p73, or Reln) (Figure 2H). This experiment confirmed that CRs are generated from *Foxj1*-expressing progenitors, consistent with recent data using a distinct *Foxj1*^{Cre} strain.[36]

We therefore concluded that CRs originating from medial sources (hem, septum, and ThE) transiently express an apparently complete gene module known to regulate multiciliation at the onset of their differentiation.

We then decided to investigate whether the expression of multiciliation genes in differentiating CRs was evolutionarily conserved. Indeed, CRs have been postulated as important players during brain evolution,[15] and the presence of CRs in the avian pallium remains a matter of debate.[1] We detected strong expression of *Gmnc* in the septum and hem regions of E5 chick embryos (Figure S2E), in direct apposition to cells expressing *Trp73*, *Ebf3*, and *Reln* located in the MZ. We concluded that the transient expression of multiciliation genes during the differentiation of CRs originating from medial sources is most likely evolutionarily conserved among amniotes.

So far, CRs have not been reported to be a multiciliated cell type. However, previous work showing that *Gmnc* expression in pallial progenitors is sufficient to induce centriole amplification, leading to the growth of multiple cilia and acquisition of an ependymal fate,[31] prompted us to investigate whether CRs could undergo multiciliation during their differentiation. We thus performed immunostaining for the centriole marker FGFR1 Oncogene Partner (FOP) on E12.5 embryos. Newly generated CRs, identified by their position in the hem and expression of p73, displayed a single FOP$^+$ foci, sometimes sufficiently resolved to distinguish a pair of centrioles (Figures 3A and 3B). In addition, flat-mount neocortical preparation of *Wnt3a*^{Cre};*Rosa26*^{tdTomato} embryos indicated that genetically identified CRs that had migrated away from the hem also bear a single pair of centrioles, contrasting with ChP from the same sample that showed robust centriolar amplification (Figures 3C and 3D). Finally, Arl13b-positive cilia above p21^{high} CR nuclei in the hem appeared well defined, short, and straight (Figure 3E), whereas their counterparts in p21^{low} ChP were found long, tortuous, and intermingled (Figure 3F). Thus, although CRs express transiently all the major known multiciliation genes, they do not undergo centriole amplification or multiciliation upon differentiation (Figure 3G).

The multiciliation master gene *Gmnc* is required for medial CR fate specification

The absence of centriolar amplification in CRs raises the question of the functional implication of the multiciliation gene

(B) GO-term analysis showing the statistical enrichment of multiciliation-related genes during CRs differentiation.
(C) SPRING representation showing the transient expression of multiciliation genes during CRs differentiation.
(D) Venn diagram highlighting the overlap between CRs- and ChP-enriched genes.
(E) Simplified view of the gene regulatory network involved in centriolar amplification and multiciliation.
(F and G) ISH on coronal sections of the E11.5 or E12.5 forebrain showing expression of multiciliation genes in the hem (F), septum, and ThE (G).
(H) Genetic tracing showing that the progeny of *Foxj1*-expressing cells (arrows) is found in the ChP, ThE and cortical marginal zone. High magnification images show selected Tomato$^+$ cells immunoreactive for CRs markers Ebf3, p73, or Reln (cells sampled from the septum, neocortex, and hem regions, respectively). At least n = 2 embryos were analyzed in (F)–(H). Scale bars: 100 μm in (F)–(H) and 20 μm in (H) (bottom). See also Figure S2 and Tables S2 and S4.

Please cite this article in press as: Moreau et al., Repurposing of the multiciliation gene regulatory network in fate specification of Cajal-Retzius neurons, Developmental Cell (2023), https://doi.org/10.1016/j.devcel.2023.05.011

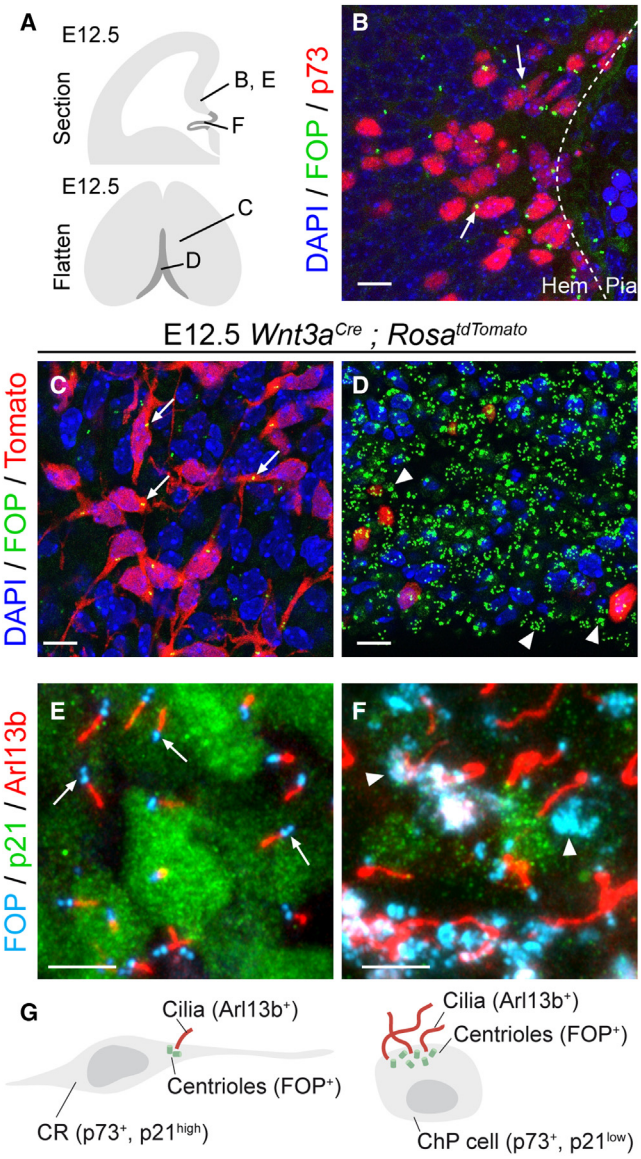

Figure 3. Centrioles and cilia in CR cells and ChP

(A) Drawing indicating the position of images in (B)–(F).

(B) Immunofluorescence for FOP (green) and p73 (red) showing a single centriole (arrows) in nascent CRs. Nuclei are stained with 4′, 6-diamidino-2-phenylindole (DAPI) (blue). The dotted line depicts the pial surface of the hem.

(C and D) En-face imaging of the neocortical surface (C) and ChP (D) showing centrioles (FOP^+, green) and hem-derived cells (Tomato+, red), corresponding to CRs (C) as well as rare ChP cells (D). CRs display a single FOP^+ foci (arrows in C), contrasting with centriolar amplification observed in ChP (arrowheads in D).

(E and F) Immunostaining of the hem (E) and ChP (F) using antibodies against FOP (cyan) and Arl13b (red) to visualize centrioles and cilia, respectively. CRs are strongly immunoreactive for p21 (green) and display one short and straight cilia growing from a single pair of centrioles (arrows in E), whereas ChP show weaker p21 expression, long and tortuous cilia as well as centriole amplification (arrowheads in F). At least 2 embryos were analyzed for each staining.

(G) Drawing summarizing the findings. Scale bars, 10 μm.

module. We therefore investigated the consequences of a complete disruption of the multiciliation regulatory network, using mouse deficient for *Gmnc*, the gene described as the most upstream regulator of the cascade[33] (Figure 2E). Of note, we initially attempted to achieve conditional deletion but failed to validate efficient recombination of the floxed *Gmnc* locus in CRs and therefore conducted all subsequent analyses using constitutive mutants.

We first performed scRNA-seq on E12.5 hem explants collected from $Gmnc^{-/-}$ embryos. After quality control and filtering, we obtained 10,036 cells with a median 3,123 genes detected per cell. SPRING dimensionality reduction displayed a topology reminiscent of the wild-type dataset, with $Sox2^+$/$Foxg1^+$ MP/DP progenitors segregated away from $Wnt3a^+$ hem, $Dlk1^+$ ThE, and Ttr^+ choroid domains (Figure S3A). Neuronal trajectories were also readily identified as $Tbr1^+$ neurons emerging from both MP/DP and Hem/ThE progenitors, suggesting normal neuronal production, although they appeared less obviously resolved than in the wild-type condition. Consistent with previous data,[29] we confirmed that *Gmnc* target genes, including *Mcidas*, *Ccno*, *Ccdc67/Deup1*, and *Trp73* were absent from the mutant dataset, whereas transcripts from the mutant *Gmnc* locus were still detectable as they retained the 3′ UTR (Figure S3B). In order to better appreciate changes upon *Gmnc* loss, we performed cell type label transfer to predict identities in the mutant dataset using the wild type as a reference, as well as dataset integration and projection of mutant cells onto the wild-type reference (Figure 4A). Although pallial, hem, ThE, and ChP progenitors were found and correctly represented in *Gmnc* mutants, not a single cell was annotated as differentiated ChP, consistent with previous reports indicating defective ChP multiciliation in $Gmnc^{-/-}$ animals.[29] However, ChP were correctly specified as indicated by the normal expression of *Ttr* or *Htr2c* (Figure S3C). Furthermore, the wild-type CR differentiation trajectory remained unmatched by mutant cells that instead occupied a position close to CP neurons in the 2D embedding (Figure 4A). To circumvent such an apparent coalescence of CR and CP neuronal trajectories in the mutant dataset, we isolated mature neurons, subjected them to unsupervised hierarchical clustering and reconstructed their lineage of origin using FateID (Figure S3D). The smallest of the three identified lineages contained the only $Lhx1^+$ cells remaining in the mutant dataset and was also characterized by the expression of ThE genes *Gm27199*, *Grm1*, *Chl1*, and *Unc5c* (Figures S3D and S3E). Since *Lhx1* expression is restricted to the ThE and ventral migratory stream in $Gmnc^{-/-}$ embryos (Figure S3F), we concluded these cells most likely correspond to ThE-derived CRs. Because of their low sampling, we excluded this small subset from subsequent analyses. Among the two remaining neuronal lineages, CP neurons were readily distinguished as $Foxg1^+$/$Prdm8^+$/$Robo3^+$ (Figure 4B). The remaining population displayed a transcriptomic signature reminiscent of CRs, characterized by the absence of *Foxg1* and high expression of *Reln*, *Lhx5, Nr2f2, Rspo3*, *Zic5*, or *Zfp503* (Figure 4B; data not shown), and was therefore annotated as such. These mutant CRs clearly diverged from their wild-type counterparts and appeared to progressively lean toward a CP fate, although not completely

Please cite this article in press as: Moreau et al., Repurposing of the multiciliation gene regulatory network in fate specification of Cajal-Retzius neurons, Developmental Cell (2023), https://doi.org/10.1016/j.devcel.2023.05.011

CellPress

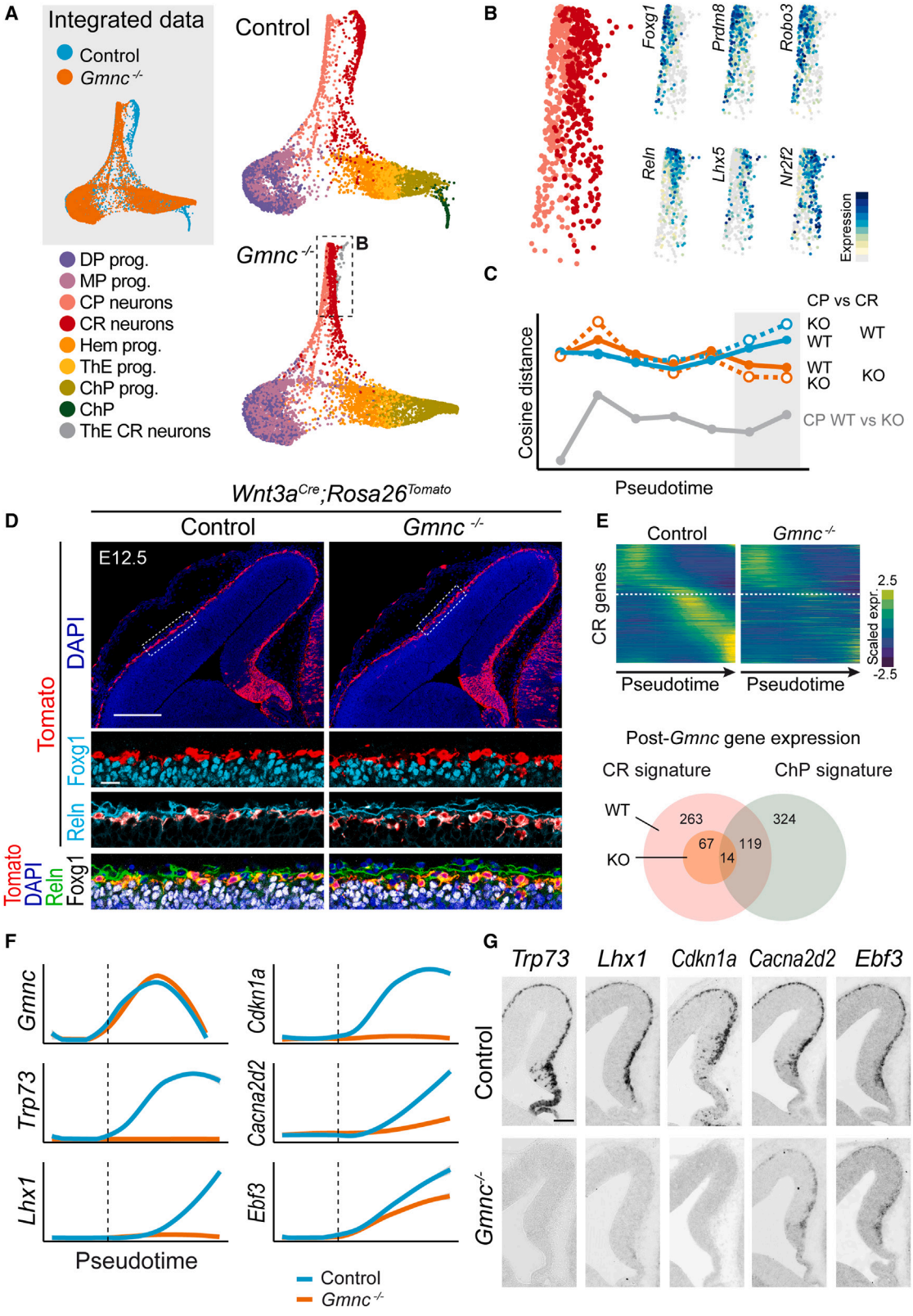

Figure 4. CR fate specification in *Gmnc* mutants

(A) SPRING embedding of integrated scRNA-seq data from control embryos and *Gmnc*$^{-/-}$ (n = 4). Cell type annotation of the mutant dataset was achieved by label transfer, using the control dataset as a reference.

(legend continued on next page)

Please cite this article in press as: Moreau et al., Repurposing of the multiciliation gene regulatory network in fate specification of Cajal-Retzius neurons, Developmental Cell (2023), https://doi.org/10.1016/j.devcel.2023.05.011

acquiring such identity as indicated by measurement of their cosine distance along pseudotime (Figure 4C).

We then performed genetic tracing using the *Wnt3a*^{Cre} driver in control and *Gmnc*$^{-/-}$ backgrounds at E12.5 to find out that regardless of the presence or absence of *Gmnc*, hem-derived cells migrate tangentially to cover the entire neocortex and remain Foxg1^{-} and Reln^{+}, all canonical features of CR fate (Figure 4D). In addition, we found the neurogenic progression, illustrated by the sequential expression of *Sox2, Neurog2*, and *Tbr1*, similar between control and mutant CR lineages (Figure S4A). Tbr2 immunostaining of the hem also indicated no difference between genotypes (Figure S4B), confirming that *Gmnc* is dispensable for CRs production. However, pseudotime analyses indicated dramatic changes in the transcriptional dynamics associated with CR differentiation, as only a small fraction of the genes normally upregulated after the onset of *Gmnc* expression were still differentially expressed in the mutant CR lineage (81 of 382, Figure 4E). The substantial overlap between CR and ChP-specific genes observed in wild-type animals was no longer present in *Gmnc* mutants (Figure 4E), indicating that most of the similarity between the two lineages corresponds to *Gmnc*-dependent genes. These results indicate that the multiciliation gene regulatory network is a strong contributor not only to ChP but also to CR identity. Consistently, classical marker genes of medial CRs, such as *Trp73*, *Lhx1*, or *Cdkn1a*, were not detected in the mutant trajectory, whereas others like *Cacna2d2* or *Ebf3* displayed decreased expression (Figure 4F). ISH experiments confirmed these findings, showing a complete loss of *Trp73, Lhx1*, and *Cdkn1a* expression, and a strong reduction of *Cacna2d2* and *Ebf3* in the neocortex of mutants (Figure 4G). Conversely, we failed to identify genes convincingly upregulated in mutant CRs, suggesting that their apparent proximity with CP neurons is not due to fate convergence but rather to a loss of the aforementioned medial signature. Taken together, these observations demonstrate a normal production but improper fate specification of CRs upon disruption of the multiciliation gene network.

Establishment of a complete identity is required for CRs survival

To investigate the consequences of CR mis-specification, we first performed ISH experiments at E13.5 in *Gmnc* mutants and control littermates. We observed a striking absence of expression of all tested marker genes of medial CR identity, including *Ebf3* or *Cacna2d2* that were still detected 1 day earlier (Figures 5A–5C and S5 compare with Figure 4G). ISH for pan-CR marker genes *Reln* or *Nhlh2* showed an almost complete loss of signal in the DP and MP of mutants (Figures 5B, 5C, and S5), whereas staining was still observed in the MZ of the lateral and ventral pallium (Figures 5B and S5). Some rare *Reln*$^{+}$ and *Nhlh2*$^{+}$ cells were found ectopically positioned deep within the CP (Figure 5C), reminiscent of mice lacking the chemokine *Cxcl12* or its receptors *Cxcr4* and *Ackr3/Cxcr7*.[37–39] Consistently, we found that *Ackr3* expression in CRs is severely impaired in *Gmnc* mutants (Figure S5C), suggesting that mis-specified cells dive in the CP because they lack normal Cxcl12/Ackr3 signaling. Whole-mount immunostaining followed by tissue clearing and light sheet imaging confirmed the drastic reduction of Reln^{+} cells in the dorsal cortex, but not the piriform region, of E14.5 mutants compared with wild-type embryos (Figure 5D). This could either result from CRs losing the expression of specific genes or reflect the absence of CRs themselves. To formally distinguish between these possibilities and address the origin of remaining Reln^{+} cells in mutants, we performed genetic tracing of hem-derived cells (*Wnt3a*^{Cre}*;Rosa26*^{tdTomato}) in control and *Gmnc*$^{-/-}$ backgrounds. At E14.5, we observed a drastic reduction in the number of Tomato^{+} cells in the DP of *Gmnc* mutants compared with control littermates (Figure 5E) or E12.5 mutants (Figure 4D), suggesting that the initial incomplete specification of CRs eventually leads to their demise. Of note, CRs remaining in the lateral and ventral pallium of *Gmnc* mutants did not invade the depleted DP at E14.5 (Figures 5B and 5E) or E18.5 (not illustrated), suggesting that self-repulsion[40] is not the only mechanism involved in the subtype-specific distribution pattern of CRs. According to *Wnt3a* genetic tracing, a small fraction of these remaining CRs derive from the hem and intermingle with Tomato^{-} CRs most likely derived from the PSB and ThE (Figures 5E and S3F).

The disappearance of hem-derived CRs in *Gmnc* mutants prompted us to investigate whether cell death occurs following mis-specification. Whole-mount TUNEL staining of E13.5 telencephalic vesicles showed an increased number of dead cells and debris in mutants compared with controls (Figure 5F). Consistently, immunostaining for activated-Caspase3 on flat-mount cortical preparations collected 1 day earlier (E12.5) indicated an increased number of cells undergoing apoptosis, most of which were also Reln^{+} (Figure 5G). We therefore concluded that upon disruption of the multiciliation gene cascade, medial CRs are produced normally, migrate tangentially, but fail to establish a complete identity and eventually trigger apoptosis.

Genetic dissection of the multiciliation gene network during CR fate specification

Gmnc was previously described as the most upstream element of the multiciliation gene regulatory network, controlling directly

(B) High magnification of (A) indicating that mutant CRs can be distinguished from CP despite their apparent coalescence, as exemplified with the expression of selected genes.

(C) Cosine distance between CRs and CP along pseudotime, the area in gray corresponds to the most differentiated states. CRs from *Gmnc* mutants (orange lines) differ less from CP than their WT relatives (blue lines), regardless of the genotype of CP (indicated by line types).

(D) Immunostaining on coronal sections of the pallium of E12.5 *Wnt3a*^{Cre}*;Rosa26*^{tdTomato} control or *Gmnc*$^{-/-}$ embryos. The magnified area is indicated by dashed lines. For both genotypes, hem-derived (Tomato^{+}) cells are found in the neocortical marginal zone and are Foxg1^{-} and Reln^{+}.

(E) Heatmap (top) showing the disruption of CRs-specific gene expression during differentiation in *Gmnc* mutants. The dashed line corresponds to *Gmnc*. Venn diagram (bottom) representing the decreased transcriptional overlap between CRs and ChP following *Gmnc* loss.

(F) Temporal expression dynamics of selected genes during CRs differentiation in control (blue) and *Gmnc*$^{-/-}$ (orange) embryos. Mutant *Gmnc* transcripts lack exons 3 and 4 but retain the 3′ UTR and are therefore detected by scRNA-seq. The dashed lines correspond to the exit of apical progenitor state.

(G) ISH on coronal sections of E12.5 embryos confirming the complete loss, or severe reduction, of expression of the CRs marker genes in *Gmnc* mutants. At least n = 2 embryos were analyzed in (D) and (G) Scale bars: 200 μm in (D); 100 μm in (G); and 20 μm in high-magnifications in (D). See also Figures S3 and S4.

Please cite this article in press as: Moreau et al., Repurposing of the multiciliation gene regulatory network in fate specification of Cajal-Retzius neurons, Developmental Cell (2023), https://doi.org/10.1016/j.devcel.2023.05.011

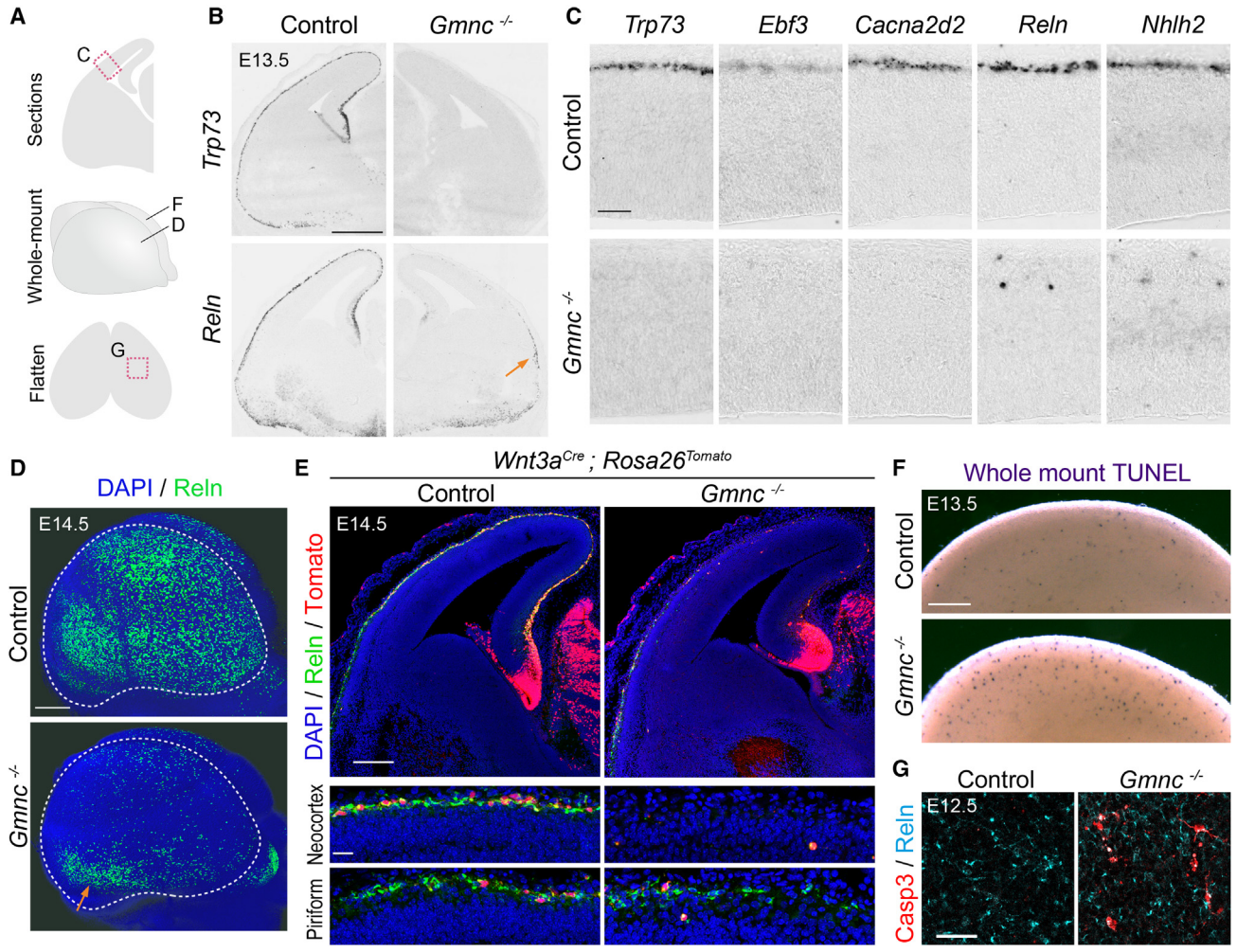

Figure 5. CR cells survival in *Gmnc* mutants

(A) Drawings indicating the regions shown in (B)–(G).

(B) ISH for *Trp73* and *Reln* showing the severe loss of signal in the dorsal cortex of E13.5 *Gmnc* mutants compared with controls. The arrow points to the remaining *Reln*$^{+}$ cells in the presumptive piriform cortex.

(C) ISH for selected genes specific of either medial (*Trp73*, *Ebf3*, and *Cacna2d2*) or all (*Reln* and *Nhlh2*) CRs subtypes in the dorsal cortex at E13.5.

(D) Light sheet microscopy showing a lateral view of the E14.5 telencephalon following Reln immunostaining (green) in control and *Gmnc* mutants. The arrow points to remaining CRs in the presumptive piriform cortex of mutants.

(E) Immunostaining of E14.5 *Wnt3a*^{Cre};*Rosa26*^{tdTomato} control or *Gmnc*$^{-/-}$ embryos showing the loss of hem-derived (Tomato^{+}, red) and Reln^{+} (green) CRs. High magnification (bottom) illustrate a segment of the neocortex and piriform cortex.

(F) Whole-mount TUNEL staining showing increased cell death in the E13.5 dorso-medial cortex of *Gmnc* mutants compared to controls.

(G) Surface view of flatten cortex preparations after immunostaining for activated caspase-3 (red) and Reln (cyan), showing increased apoptosis in E12.5 *Gmnc*$^{-/-}$ embryos relative to wild types. At least n = 2 embryos were analyzed. Scale bars: 500 μm in (B) and (D); 200 μm in (E) and (F); 50 μm in (C) and (G); and 20 μm in high magnification in (E). See also Figure S5.

or indirectly the expression of all other effectors.[33] To test whether such effectors are involved in CR specification, we analyzed their contribution using mouse mutants collected at E13.5, a stage at which *Gmnc* deficiency leads to a robust CRs depletion from the dorsal cortex.

Trp73 is a known player in multiciliation and a direct target of *Gmnc*.[30] In addition, a severe reduction of Reln^{+} cells in the cortex and hippocampus of mice lacking *Trp73* has already been reported.[41] We subjected E13.5 forebrain sections from *Trp73*$^{-/-}$ embryos to ISH using probes directed against pan-CR marker genes *Reln* and *Nhlh2*, as well as medial CR markers *Lhx1* and *Cacna2d2*. We observed a phenotype highly reminiscent of *Gmnc* mutants, consisting in the complete absence of *Lhx1* and *Cacna2d2* expression in the DP (Figure 6B), the preservation of *Reln*$^{+}$/*Nhlh2*$^{+}$ cells in the lateral/ventral pallium (Figure S6A), the occurrence of ectopic *Reln*$^{+}$/*Nhlh2*$^{+}$ cells deep into the CP (Figure S6B), and the presence of numerous apoptotic cell bodies in the MZ (Figures S6C and S6D). These data suggest that the loss of *Trp73* expression phenocopies that of *Gmnc*, at least for what concerns the establishment and maintenance of medial CR identity. The *Trp73* gene gives rise to several functionally different isoforms depending on alternative

Please cite this article in press as: Moreau et al., Repurposing of the multiciliation gene regulatory network in fate specification of Cajal-Retzius neurons, Developmental Cell (2023), https://doi.org/10.1016/j.devcel.2023.05.011

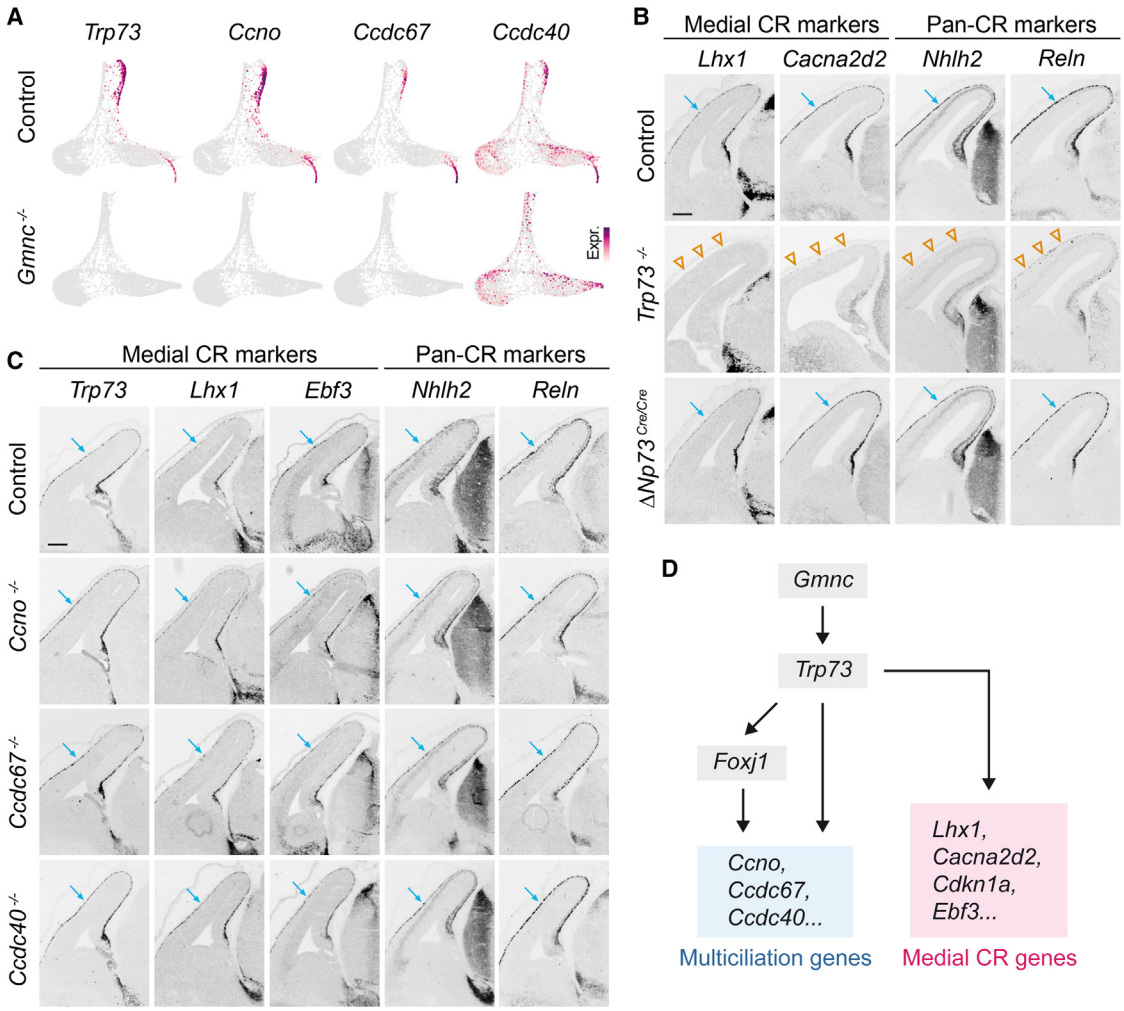

Figure 6. Contribution of multiciliation genes to CR fate specification

(A) SPRING embedding showing the expression of selected genes whose expression is lost, or severely affected, in *Gmnc*$^{-/-}$ CRs.

(B) ISH for CRs marker genes (derived from medial sources, or all subtypes) in E13.5 knockout embryos with complete deficiency of p73, or with specific inactivation of the ΔNp73 isoform. Blue arrows indicate normal staining in the marginal zone. Orange arrowheads indicate the absence of staining in *Trp73* mutants. Scale bars, 200 μm.

(C) ISH for CRs marker genes in E13.5 embryos deficient for *Ccno*, *Ccdc67*, or *Ccdc40*. Controls and mutants could not be distinguished. Blue arrows indicate normal staining in the marginal zone. At least 2 embryos per genotype analyzed. Scale bars, 200 μm.

(D) Diagram summarizing the proposed contribution of *Gmnc* effectors to CRs differentiation. Multiciliation genes (blue) are dispensable for the induction of medial CR genes (red). See also Figure S6.

promoters[42,43]: a transcriptionally active protein, referred to as TAp73, and a variant lacking the N-terminal transactivation domain named ΔNp73. Mouse mutants in which a Cre-IRES-EGFP cassette was inserted just after the initiation codon of ΔNp73 display an apparent normal number of GFP^{+} cells at E11.5, which progressively decrease to approximately 50% of controls at P0,[21] suggesting a normal production but abnormal survival of CRs in the absence of ΔNp73. To further study CR fate specification and acquisition of medial identity in these mutants, we performed ISH experiments for pan-CR (*Reln* and *Nhlh2*) and medial CR marker genes (*Lhx1* and *Cacna2d2*). At E13.5, all these genes were specifically expressed in the cortical MZ (Figure 6B), showing that ΔNp73 is dispensable for the initial acquisition of medial CR fate. Our observations suggest that hem-derived CRs acquire their medial identity through the *Gmnc*-dependent activation of *Trp73* and specially point to TAp73 as the responsible isoform.

We further dissected the contribution of *Gmnc* effectors to CR fate specification. *Ccno* is a known *Gmnc* target required for multiciliogenesis.[29,44–46] *Ccdc67/Deup1* is also a target of *Gmnc*, essential for the assembly of deuterosome, although its precise function during centriolar amplification and multiciliation remains debated.[47,48] Since both *Ccno* and *Ccdc67* were found absent in the CR trajectory of *Gmnc* mutants (Figure 6A), we analyzed brains obtained from E13.5 embryos lacking either gene to find out that, in both cases, CR markers *Trp73*, *Lhx1*,

Please cite this article in press as: Moreau et al., Repurposing of the multiciliation gene regulatory network in fate specification of Cajal-Retzius neurons, Developmental Cell (2023), https://doi.org/10.1016/j.devcel.2023.05.011

CellPress

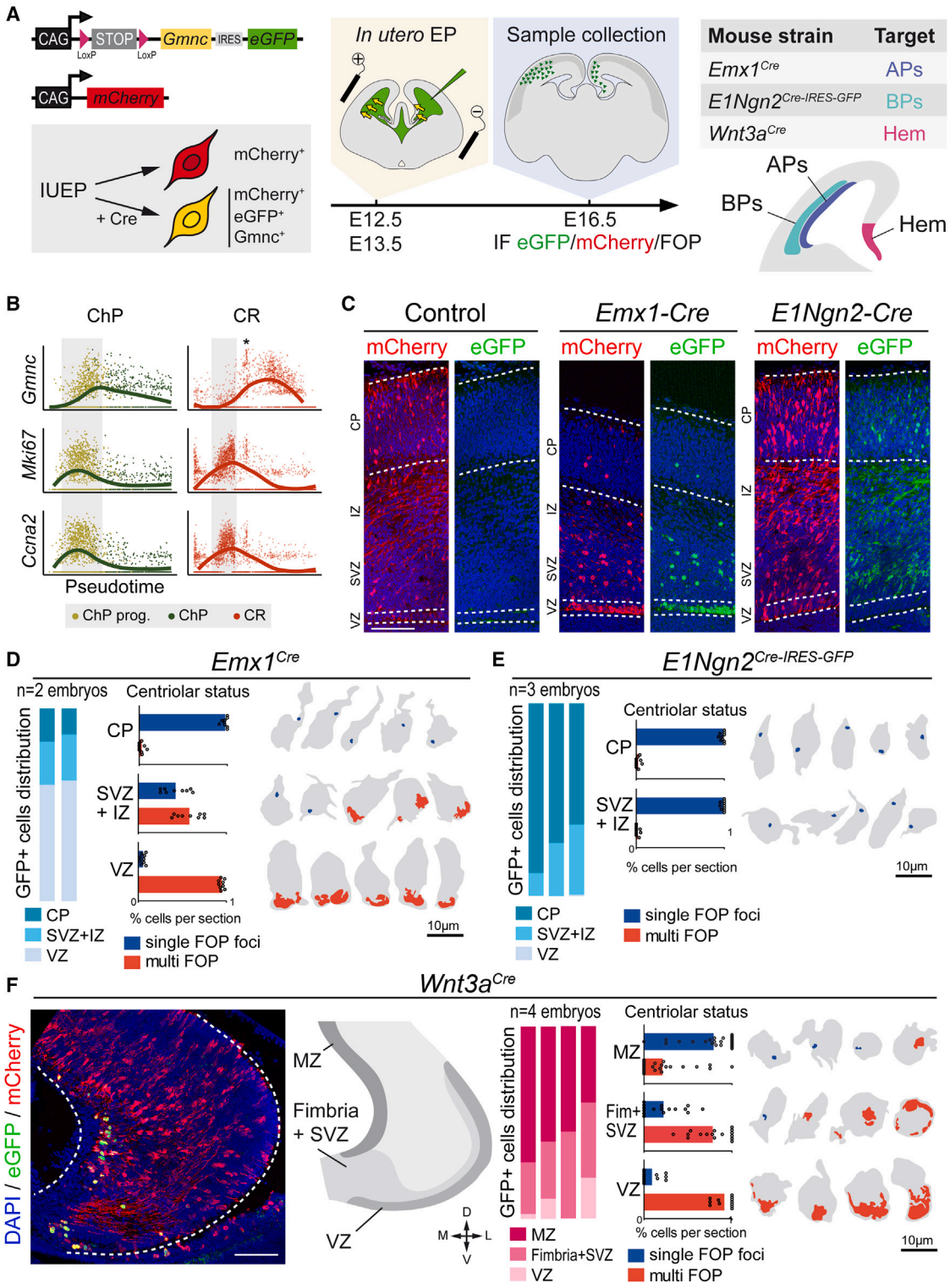

Figure 7. Context-dependent response to *Gmnc* expression

(A) Plasmids allowing Cre-dependent expression of *Gmnc* together with e*GFP*, and the constitutive expression of *mCherry* were combined to monitor both electroporated cells and *Gmnc*-expressing cells. *In utero* electroporation experiments were conducted in *Emx1*^{Cre}, *E1Ngn2*^{Cre}, or *Wnt3a*^{Cre} embryos to selectively target apical (APs), basal (BPs) or hem progenitors, respectively.

(B) Temporal dynamics of *Gmnc* expression compared to that of cell cycle genes *Mki67* and *Ccna2* during ChP (left) or CR (right) differentiation. The area in gray corresponds to S/G2/M phases, the asterisk indicates cycling BPs.

(legend continued on next page)

Please cite this article in press as: Moreau et al., Repurposing of the multiciliation gene regulatory network in fate specification of Cajal-Retzius neurons, Developmental Cell (2023), https://doi.org/10.1016/j.devcel.2023.05.011

Ebf3, *Nhlh2*, and *Reln* were normally expressed in the DP (Figure 6C).

Finally, we tested whether genes known to control cilia motility and shared by CRs and ChP were required for CR fate. We focused on *Ccdc40* as we found its expression affected in *Gmnc* mutants (Figure 6A). We subjected E13.5 brain sections from *Ccdc40*$^{-/-}$ embryos to ISH using probes for *Trp73*, *Lhx1*, *Ebf3*, *Nhlh2*, *and Reln* to find out that medial CR identity is correctly acquired (Figure 6C).

From these experiments, we concluded that *Trp73* is an essential player for CR fate specification downstream *Gmnc*, whereas other tested components of the gene regulatory network are dispensable, at least for the initial acquisition of CR identity (Figure 6D). Therefore, despite the significant overlap in their transcriptomic signatures, CRs and ChP differentially interpret the expression of *Gmnc*.

Expression dynamics and regional cues influence *Gmnc*-induced centriolar amplification

Gmnc has been reported to be a strong inducer of multiciliation. The absence of centriolar amplification in CRs, together with the differential requirement of *Gmnc* downstream effectors in CRs vs. multiciliated tissues, raise the question of how the same gene can perform drastically distinct functions in CR and multiciliated lineages.

To determine if the cellular context may influence the ability of *Gmnc* to initiate multiciliation, we implemented *in utero* electroporation experiments. Using this assay, it was shown that the ectopic expression of *Gmnc* in neocortical apical progenitors induces a strong centriolar amplification and retention of electroporated cells at the ventricular surface, reminiscent of ependymal cells, instead of undergoing neuronal differentiation and radial migration toward the pia.[25,31,49]

We noticed that the dynamics of *Gmnc* expression differs along ChP and CR differentiation trajectories. In ChP, *Gmnc* expression is initiated in cycling apical progenitor, whereas in CRs, it rather starts at the exit of apical progenitor state and peaks in basal/intermediate progenitors (Figure 7B). This was confirmed at the tissue level as *Gmnc* mRNA expression was found to robustly overlap with Tbr2 immunolabeling in the hem and ThE (Figure S7A). In order to test whether heterochrony in *Gmnc* expression could restrict its ability to induce multiciliation, we electroporated a LoxP-Stop-LoxP-*Gmnc* construct in *E1-Ngn2*^{Cre} embryos to specifically target basal progenitors and compared with inducing expression in apical progenitors using *Emx1*^{Cre} (Figure 7A). Electroporation was performed at E12.5 or E13.5 and brains collected at E16.5, i.e., prior to the initiation of endogenous *Gmnc* expression in prospective ependymal cells of the targeted region.[31] As expected, electroporations in *Emx1*^{Cre} recapitulated constitutive *Gmnc* expression in wild-type animals, with most recombined cells (~60%) found in the ventricular zone (VZ) and displaying large FOP^{+} patches characteristic of centriolar amplification (Figures 7C, 7D, and S7B) as well as multiple Arl13b^{+} cilia (Figure S7C). By contrast, the few cells (~15%) that reached the CP almost systematically showed one small FOP^{+} foci, indicating an absence of centriolar amplification. By contrast, recombined cells in *E1-Ngn2*^{Cre} embryos were mostly (~75%) found in the CP and almost never showed centriolar amplification (Figures 7E and S7B). We therefore concluded that *Gmnc* expression dynamics, especially the differentiation state at which it peaks, is a key determinant of the cellular response it triggers, consistent with recent findings showing that multiciliation occurs only when *Gmnc* is expressed in cycling progenitors.[25]

Finally, we tested whether the region of expression could also control the response to *Gmnc*. Since apical progenitors of the hem differ from their relatives in the DP (see Figures 1B–1D, S1E, and S1F), we compared the consequence of *Gmnc* expression in these two domains. Electroporation of the floxed *Gmnc* construct in *Wnt3a*^{Cre} embryos resulted in much less ventricular retention of recombined cells than in *Emx1*^{Cre} embryos, indicating that apical progenitors in the hem respond differently to *Gmnc* expression than their DP counterparts (Figure 7F). Similar to both *Emx1*^{Cre} and *E1-Ngn2*^{Cre} conditions, we found centriolar amplification to occur in the progenitor rather than post-mitotic compartment (Figures 7F and S7B). Overall, we concluded that both *Gmnc* expression dynamics and hem-specific features contribute to the competence to undergo centriolar amplification or not.

Taken together, our data indicate that components of a well-conserved regulatory gene network involved in centriolar amplification and multiciliation are also essential for the fate specification of CRs derived from medial sources (hem, septum, and ThE). We propose that CR fate results from the combination of *Gmnc*-independent processes, sufficient to ensure initial production, tangential migration, and *Reln/Nhlh2* expression, together with *Gmnc*-dependent mechanisms that enable the acquisition of complete identity and survival. Our work therefore exemplifies how the co-option of a gene module, and redeployment to perform an alternative function, may result in cell type diversification.

DISCUSSION

In this study, we unveil the developmental process involved in the fate specification of medial CRs. Focusing on the major source, the cortical hem, we performed scRNA-seq and reconstructed the CR differentiation trajectory to unravel a transient expression of the whole gene module controlling multiciliation.

(C) Immunostaining of the dorsal cortex showing the position of electroporated (mCherry^{+}, red) and *Gmnc*-expressing cells (eGFP^{+}, green). Dashed lines indicate the regions considered for quantifications. Scale bar, 100 μm.

(D and E) Quantification of *Gmnc*-expressing cells distribution and centriole amplification after *in utero* electroporation in *Emx1*^{Cre} (D) or *E1Ngn2*^{Cre} (E) embryos. Gray shapes shown next to the histograms correspond to cells representative of each region in which the pattern of FOP staining is represented in blue or red according to the centriolar status. Original images are shown in Figure S7B. Scale bars, 10 μm.

(F) *In utero* electroporation in *Wnt3a*^{Cre} embryos. Immunostaining of the hem region showing electoroporated (mCherry^{+}, red) and *Gmnc*-expressing cells (eGFP^{+}, green). Scale bar, 100 μm. The drawing indicates the regions considered for quantifications. Quantification and representative FOP patterns are shown as in (D) and (E). 1,706 cells were counted from 9 sections of 2 embryos in (D), 588 cells from 10 sections of 3 embryos in (E), and 310 cells from 27 sections of 4 embryos in (F). VZ, ventricular zone; SVZ, subventricular zone; IZ, intermediate zone; CP, cortical plate; MZ, marginal zone. See also Figure S7.

Please cite this article in press as: Moreau et al., Repurposing of the multiciliation gene regulatory network in fate specification of Cajal-Retzius neurons, Developmental Cell (2023), https://doi.org/10.1016/j.devcel.2023.05.011

Our results, hence, uncover the close relationship between medial CR fate specification and acquisition of the multiciliated phenotype of ChP.

The shared expression of *Trp73* by CRs and ChP, and the continuity of their progenitor domains have long suggested a link between their development.[21,50–53] The relationship between CR and ChP fate specification in the telencephalic midline was previously investigated by Imayoshi et al.[54] In their study, they showed that *Hes1/3/5*-mediated repression of *Neurog2* is required for ChP specification since their combined loss of function leads to the overproduction of CRs at the expense of ChP.[54] Furthermore, ChP to CRs conversion was also observed upon *Neurog2* gain of function at early (E9.5) but not late (E11.5) stages of midline patterning, suggesting that progenitors for each lineage are segregated and fully committed by E11.5. Supporting this observation, our data show a clear distinction between CR and ChP progenitors both at E11.5 and E12.5, arguing against the existence of CR/ChP bipotent progenitors at this stage.

The cortical hem is the major source of neocortical CRs in the mouse.[19] It acts as a signaling center and is considered part of the telencephalon; however, our data clearly highlight the significant transcriptional gap with MP/DP progenitor pools. Interestingly, although the hem, septum, and ThE have been studied as independent structures, their molecular identities share some fundamental features that lead to the proposal that they rather represent a continuum referred to as the forebrain-hem system.[52] Progenitors of the forebrain-hem system express the transcription factors *Id3*, *Otx2*, and *Zic2*[34,52,55] and their identity is repressed by the pallial transcription factors *Lhx2* and *Foxg1*.[52,56–59] Therefore, the very distinctive transcriptomic signature of CRs, illustrated by their systematic divergence from other cortical excitatory neurons in scRNA-seq datasets,[1] likely stems from the equally unique identity of their progenitors. In this line, lineage tracing experiments recently demonstrated that neocortical and hippocampal CRs derive from progenitors that are already fate-restricted at E9.5.[60]

Multiciliated ChP and ependymal cells are well conserved among vertebrates[61,62] and the *Gmnc*-dependent multiciliation regulatory network is also shared by vertebrates,[63] suggesting their coevolution. By contrast, CRs have not been described beyond amniotes so far, suggesting that they represent a relatively recent evolutionary innovation. We provide strong evidence supporting the existence of CRs in chicks, matching previous observations made in lizards and crocodiles[64,65] and confirming that CR identity was already present in the last common ancestor of amniotes at least. Nevertheless, our observation that CR fate specification relies on the multiciliation gene module supports a scenario whereby *Gmnc* expression expanded from an ancestral ChP domain into the neighboring tissue of the forebrain-hem system with distinct dynamics and was differentially interpreted. Further studies will be necessary to validate such a hypothesis and understand the mechanisms regulating *Gmnc* expression in space and time.

How the same gene module can control two very distinct biological processes remains a puzzling question. During the course of this study, we investigated the possibility that the alternative functions of *Gmnc* in CRs and multiciliated lineages could be due to a partial co-option of its downstream regulatory network. However, we failed to identify convincing differences in the expression of known *Gmnc* effectors between CRs and ChP. Investigating the influence of the cellular context proves more successful, with the demonstration that the cell state and territory in which *Gmnc* is expressed can influence its ability to trigger centriole amplification, which is the first step toward assembling multiple motile cilia.[66] The heterochrony of *Gmnc* expression in CRs vs. ChP, and its demonstrated impact on centriole amplification corroborate recent work showing that *Gmnc* expression in cortical progenitors favors ependymal fate[49] and that *Gmnc* induces multiciliation only when expressed in cycling cells.[25] By contrast, why hem and DP progenitors are not equally competent remains an open question. Multiple transcription factors are differentially expressed between apical progenitors of these two domains (Figure S1F) and could account for their distinct response to *Gmnc* expression. Among these, *Foxg1* is an appealing candidate as it was shown to prevent CR fate.[23,24] We propose that CR specification results from the initial absence of *Foxg1* at the apical progenitor state, followed by the recruitment of the multiciliation regulatory network upon cell cycle exit to progress toward a fully differentiated and viable state without triggering centriole amplification.

The two opposite functional outcomes of the *Gmnc* module in CRs and ChP suggest different target genes are at play in the two lineages. We showed that *Gmnc* mutant phenotype in medial CRs is phenocopied by the loss of *Trp73*, indicating that *Gmnc* function in CR fate specification is mediated by *Trp73*, consistent with previous reports.[41,42,50,67] Interestingly, *Trp73* is a key player in ependymal specification, maturation, and organization.[68–70] It is also a well-known regulator of multiciliation through its direct control on the transcription of key effector genes.[26,71] Although further work will be required to identify *Trp73* targets in CRs vs. ChP, it is tempting to speculate that the co-option of *Trp73* by CRs has been followed by the acquisition of new target genes, leading to a functional divergence from ChP.

CRs have a transient lifetime,[72–74] previously prompting us to postulate that they could be fated to die.[75] In this frame, our observation that mis-specified CRs undergo premature apoptosis in *Gmnc* and *Trp73* mutants suggests that acquisition of their complete identity is required to maintain them alive. Such a hypothesis is supported by the demonstrated role of ΔNp73 in the survival of CRs.[21] It also raises the question of PSB-derived CRs that never express *Gmnc* or *Trp73*. One could speculate that their similarity with mis-specified medial CRs in *Gmnc* mutants foretells a short lifetime, supporting further investigations to precisely determine the survival curve of PSB-derived CRs.

CRs represent a rare but very important cell type in the developing neocortex, involved in multiple aspects of its morphogenesis, and proposed to contribute to its tremendous expansion and complexification in mammals.[1,15] We believe that our work exemplifies how the co-option of a single gene, followed by the refunctionalization of its downstream regulatory network, may result in the invention of a novel cell type, and how cell type diversification can occur by dramatic leap rather than progressive divergence.

Limitations of the study

One technical limitation we faced was the inefficient recombination that prevented us from using CR-specific conditional inactivation of *Gmnc*. We therefore cannot totally and formally exclude that

some of the defects are non-cell-autonomous, although we have no reason to believe this is the case. Because CRs are such important players in cortical development, one obvious limitation is that we did not investigate the consequences of the massive CR depletion observed in *Gmnc* mutants on cortical morphogenesis, especially layer formation. This is deliberate, as we believe that such a question cannot be properly addressed here because of space limitations and deserves a dedicated study. Our electroporation experiments indicate that both the timing and region of *Gmnc* expression influence its ability to induce mutliciliogenesis. However, we did not explain why this is the case. What are the regulatory elements driving *Gmnc* expression in CR vs. ChP? What are the lineage-specific *Gmnc* co-factors? For now, these questions remain unresolved. Finally, we believe that our findings are highly relevant for cortical evolution and cell types diversification. However, the evolutionary implications of our work are not fully resolved here. A definitive conclusion on the mechanisms that enabled the co-option and repurposing of the multiciliogenesis gene regulatory network, and the evolutionary emergence of CRs would require studying additional species in detail.

STAR★METHODS

Detailed methods are provided in the online version of this paper and include the following:

- KEY RESOURCES TABLE
- RESOURCE AVAILABILITY
  - Lead contact
  - Materials availability
  - Data and code availability
- EXPERIMENTAL MODEL AND STUDY PARTICIPANT DETAILS
  - Mouse strains
- METHOD DETAILS
  - scRNAseq
  - Cell filtering
  - Broad clustering and cell type annotation
  - Trajectories
  - ScRNAseq atlas analysis
  - Cloning
  - Electroporation
  - Tissue processing
  - Tissue clearing
  - Immunostaining
  - *In situ* hybridisation
  - Whole mount TUNEL staining
  - Image acquisition
- QUANTIFICATION AND STATISTICAL ANALYSIS
- ADDITIONAL RESOURCES

SUPPLEMENTAL INFORMATION

Supplemental information can be found online at https://doi.org/10.1016/j.devcel.2023.05.011.

ACKNOWLEDGMENTS

The authors thank Marine Luka and the LabTech Single-Cell@Imagine as well as Cecile Masson and the Imagine Institute genomic and bioinformatics platforms for their help with scRNA-seq. We are grateful to Francesco Carbone and Jérôme Flatot for implementing the Shiny App server, and to Institut Français de Bioinformatique for access to the IFB-core cluster. We acknowledge the histology and imaging facilities of the SFR Necker (Inserm US24, CNRS UAR3633) and the NeurImag facility of IPNP. We thank Leducq establishment for funding the Leica SP8 confocal/STED 3DX system at IPNP and Association pour la Recherche sur le Cancer for funding the Nanozoomer slide scanner at SFR Necker. We are grateful to Sébastien Dupichaud for his help with light sheet microscopy. We acknowledge the Imagine Institute LEAT and IPNP animal facility for animal care, especially the zootechnicians in charge of our colonies. We thank Sigolène Meilhac and Anna-Katerina Hadjantonakis for providing *Ccdc40/lnks* mutants. We are grateful to all members of the Pierani and Spassky labs for stimulating and helpful discussions, and Pierre Billuart for critical reading of the manuscript. M.X.M. was funded by École Normale Supérieure and Fondation pour la Recherche Médicale (FDT201904008366). A.O.-S. is a laureate from the Pasteur-Paris University (PPU) International PhD Program. L.M.-A. is the recipient of a Margarita Salas post-doctoral fellowship. This work was supported by IdEx Université Paris Cité (ANR-18-IDEX-0001), state funding from the Agence Nationale de la Recherche under the "Investissements d'avenir" program (ANR-10-IAHU-01) to the Imagine Institute, a grant from the Spanish Ministerio de Ciencia e Innovación and co-financed by FEDER funds (PID2019-105169RB-I00) to M.C.M., grants from Agence Nationale de la Recherche (ANR-19-CE16-0017-03) and the Fondation pour la Recherche Médicale (Équipe FRM EQU201903007836) to A.P., and grants from IdEx Université Paris Cité "Émergence" program (IDEX RM27J21IDXA7_CAJALIDENT) and Agence Nationale de la Recherche (ANR-22-CE16-0011-01) to F.C.

AUTHOR CONTRIBUTIONS

Conceptualization, M.X.M., N.S., A.P., and F.C.; methodology, M.X.M., Y.S., F.C., N.S., A.P., and F.C.; software, M.X.M. and F.C.; validation, M.X.M., Y.S., V.E., B.B., E.D., T.D.G., N.S., and F.C.; formal analysis, M.X.M.; investigation, M.X.M., Y.S., V.E., B.B., E.D., T.D.G., N.S., and F.C.; resources, A.O.-S., L.M.-A., M.M.M., M.C.M., and N.S.; data curation, M.X.M. and F.C.; writing—original draft, M.X.M. and F.C.; writing—review and editing, M.X.M., N.S., A.P., and F.C.; visualization, M.X.M., Y.S., V.E., B.B., E.D., N.S., and F.C.; supervision, F.C.; project administration, F.C.; funding acquisition, A.P. and F.C.

DECLARATION OF INTERESTS

The authors declare no competing interests

INCLUSION AND DIVERSITY

We support inclusive, diverse, and equitable conduct of research. One or more of the authors of this paper self-identifies as a member of the LGBTQIA+ community. One or more of the authors of this paper self-identifies as an underrepresented ethnic minority in their field of research or within their geographical location. One or more of the authors of this paper received support from a program designed to increase minority representation in their field of research.

Received: November 23, 2022
Revised: April 6, 2023
Accepted: May 19, 2023
Published: June 14, 2023

REFERENCES

1. Causeret, F., Moreau, M.X., Pierani, A., and Blanquie, O. (2021). The multiple facets of Cajal-Retzius neurons. Development *148*. dev199409. https://doi.org/10.1242/dev.199409.
2. Elorriaga, V., Pierani, A., and Causeret, F. (2023). Cajal-retzius cells: recent advances in identity and function. Curr. Opin. Neurobiol. *79*. 102686. https://doi.org/10.1016/j.conb.2023.102686.

3. Martínez-Cerdeño, V., and Noctor, S.C. (2014). Cajal, Retzius, and Cajal-Retzius cells. Front. Neuroanat. *8*, 48. https://doi.org/10.3389/fnana.2014.00048.

4. Gil, V., Nocentini, S., and Del Río, J.A. (2014). Historical first descriptions of Cajal-Retzius cells: from pioneer studies to current knowledge. Front. Neuroanat. *8*, 32. https://doi.org/10.3389/fnana.2014.00032.

5. Vílchez-Acosta, A., Manso, Y., Cárdenas, A., Elias-Tersa, A., Martínez-Losa, M., Pascual, M., Álvarez-Dolado, M., Nairn, A.C., Borrell, V., and Soriano, E. (2022). Specific contribution of Reelin expressed by Cajal–Retzius cells or GABAergic interneurons to cortical lamination. Proc. Natl. Acad. Sci. USA *119*, e2120079119. https://doi.org/10.1073/pnas.2120079119.

6. Griveau, A., Borello, U., Causeret, F., Tissir, F., Boggetto, N., Karaz, S., and Pierani, A. (2010). A novel role for Dbx1-derived Cajal-Retzius cells in early regionalization of the cerebral cortical neuroepithelium. PLoS Biol. *8*, e1000440. https://doi.org/10.1371/journal.pbio.1000440.

7. Barber, M., Arai, Y., Morishita, Y., Vigier, L., Causeret, F., Borello, U., Ledonne, F., Coppola, E., Contremoulins, V., Pfrieger, F.W., et al. (2015). Migration speed of Cajal-Retzius cells modulated by vesicular trafficking controls the size of higher-order cortical areas. Curr. Biol. *25*, 2466–2478. https://doi.org/10.1016/j.cub.2015.08.028.

8. Riva, M., Genescu, I., Habermacher, C., Orduz, D., Ledonne, F., Rijli, F.M., López-Bendito, G., Coppola, E., Garel, S., Angulo, M.C., et al. (2019). Activity-dependent death of transient cajal-retzius neurons is required for functional cortical wiring. eLife *8*, e50503. https://doi.org/10.7554/eLife.50503.

9. de Frutos, C.A., Bouvier, G., Arai, Y., Thion, M.S., Lokmane, L., Keita, M., Garcia-Dominguez, M., Charnay, P., Hirata, T., Riethmacher, D., et al. (2016). Reallocation of olfactory cajal-retzius cells shapes neocortex architecture. Neuron *92*, 435–448. https://doi.org/10.1016/j.neuron.2016.09.020.

10. Genescu, I., Aníbal-Martínez, M., Kouskoff, V., Chenouard, N., Mailhes-Hamon, C., Cartonnet, H., Lokmane, L., Rijli, F.M., López-Bendito, G., Gambino, F., et al. (2022). Dynamic interplay between thalamic activity and Cajal-Retzius cells regulates the wiring of cortical layer 1. Cell Rep. *39*, 110667. https://doi.org/10.1016/j.celrep.2022.110667.

11. Anstötz, M., Lee, S.K., and Maccaferri, G. (2022). Glutamate released by Cajal-Retzius cells impacts specific hippocampal circuits and behaviors. Cell Rep. *39*. 110822. https://doi.org/10.1016/j.celrep.2022.110822.

12. Riva, M., Moriceau, S., Morabito, A., Dossi, E., Sanchez-Bellot, C., Azzam, P., Navas-Olive, A., Gal, B., Dori, F., Cid, E., et al. (2023). Aberrant survival of hippocampal Cajal-Retzius cells leads to memory deficits, gamma rhythmopathies and susceptibility to seizures in adult mice. Nat. Commun. *14*, 1531. https://doi.org/10.1038/s41467-023-37249-7.

13. Ogawa, M., Miyata, T., Nakajima, K., Yagyu, K., Seike, M., Ikenaka, K., Yamamoto, H., Mikoshiba, K., Nakajimat, K., and Yagyu, K. (1995). The reeler gene-associated antigen on Cajal-Retzius neurons is a crucial molecule for laminar organization of cortical neurons. Neuron *14*, 899–912. https://doi.org/10.1016/0896-6273(95)90329-1.

14. D'Arcangelo, G., Miao, G.G., Chen, S.C., Soares, H.D., Morgan, J.I., and Curran, T. (1995). A protein related to extracellular matrix proteins deleted in the mouse mutant reeler. Nature *374*, 719–723. https://doi.org/10.1038/374719a0.

15. Goffinet, A.M. (2017). The evolution of cortical development: the synapsid-diapsid divergence. Development *144*, 4061–4077. https://doi.org/10.1242/dev.153908.

16. Takiguchi-Hayashi, K., Sekiguchi, M., Ashigaki, S., Takamatsu, M., Hasegawa, H., Suzuki-Migishima, R., Yokoyama, M., Nakanishi, S., and Tanabe, Y. (2004). Generation of reelin-positive marginal zone cells from the caudomedial wall of telencephalic vesicles. J. Neurosci. *24*, 2286–2295. https://doi.org/10.1523/JNEUROSCI.4671-03.2004.

17. Hevner, R.F., Neogi, T., Englund, C., Daza, R.A., and Fink, A. (2003). Cajal–Retzius cells in the mouse: transcription factors, neurotransmitters, and birthdays suggest a pallial origin. Brain Res. Dev. Brain Res. *141*, 39–53. https://doi.org/10.1016/S0165-3806(02)00641-7.

18. Bielle, F., Griveau, A., Narboux-Nême, N., Vigneau, S., Sigrist, M., Arber, S., Wassef, M., and Pierani, A. (2005). Multiple origins of Cajal-Retzius cells at the borders of the developing pallium. Nat. Neurosci. *8*, 1002–1012. https://doi.org/10.1038/nn1511.

19. Yoshida, M., Assimacopoulos, S., Jones, K.R., and Grove, E.A. (2006). Massive loss of Cajal-Retzius cells does not disrupt neocortical layer order. Development *133*, 537–545. https://doi.org/10.1242/dev.02209.

20. Ruiz-Reig, N., Andrés, B., Huilgol, D., Grove, E.A., Tissir, F., Tole, S., Theil, T., Herrera, E., and Fairén, A. (2017). Lateral thalamic eminence: A novel origin for mGluR1/lot cells. Cereb. Cortex *27*, 2841–2856. https://doi.org/10.1093/cercor/bhw126.

21. Tissir, F., Ravni, A., Achouri, Y., Riethmacher, D., Meyer, G., and Goffinet, A.M. (2009). DeltaNp73 regulates neuronal survival in vivo. Proc. Natl. Acad. Sci. USA *106*, 16871–16876. https://doi.org/10.1073/pnas.0903191106.

22. Moreau, M.X., Saillour, Y., Cwetsch, A.W., Pierani, A., and Causeret, F. (2021). Single-cell transcriptomics of the early developing mouse cerebral cortex disentangle the spatial and temporal components of neuronal fate acquisition. Development *148*. dev197962. https://doi.org/10.1242/dev.197962.

23. Hanashima, C., Li, S.C., Shen, L., Lai, E., and Fishell, G. (2004). Foxg1 suppresses early cortical cell fate. Science *303*, 56–59. https://doi.org/10.1126/science.1090674.

24. Hanashima, C., Fernandes, M., Hebert, J.M., and Fishell, G. (2007). The role of Foxg1 and dorsal midline signaling in the generation of cajal-retzius subtypes. J. Neurosci. *27*, 11103–11111. https://doi.org/10.1523/JNEUROSCI.1066-07.2007.

25. Ortiz-Álvarez, G., Fortoul, A., Srivastava, A., Moreau, M.X., Bouloudi, B., Mailhes-Hamon, C., Delgehyr, N., Faucourt, M., Bahin, M., Blugeon, C., et al. (2022). p53/p21 pathway activation contributes to the ependymal fate decision downstream of GemC1. Cell Rep. *41*. 111810. https://doi.org/10.1016/j.celrep.2022.111810.

26. Marshall, C.B., Mays, D.J., Beeler, J.S., Rosenbluth, J.M., Boyd, K.L., Santos Guasch, G.L., Shaver, T.M., Tang, L.J., Liu, Q., Shyr, Y., et al. (2016). p73 is required for multiciliogenesis and regulates the Foxj1-associated gene network. Cell Rep. *14*, 2289–2300. https://doi.org/10.1016/j.celrep.2016.02.035.

27. Spassky, N., and Meunier, A. (2017). The development and functions of multiciliated epithelia. Nat. Rev. Mol. Cell Biol. *18*, 423–436. https://doi.org/10.1038/nrm.2017.21.

28. Lun, M.P., Monuki, E.S., and Lehtinen, M.K. (2015). Development and functions of the choroid plexus-cerebrospinal fluid system. Nat. Rev. Neurosci. *16*, 445–457. https://doi.org/10.1038/nrn3921.

29. Terré, B., Piergiovanni, G., Segura-Bayona, S., Gil-Gómez, G., Youssef, S.A., Attolini, C.S.-O., Wilsch-Bräuninger, M., Jung, C., Rojas, A.M., Marjanović, M., et al. (2016). GEMC1 is a critical regulator of multiciliated cell differentiation. EMBO J. *35*, 942–960. https://doi.org/10.15252/embj.201592821.

30. Lalioti, M.-E., Arbi, M., Loukas, I., Kaplani, K., Kalogeropoulou, A., Lokka, G., Kyrousi, C., Mizi, A., Georgomanolis, T., Josipovic, N., et al. (2019). GemC1 governs multiciliogenesis through direct interaction with and transcriptional regulation of p73. J. Cell Sci. *132*. https://doi.org/10.1242/jcs.228684.

31. Kyrousi, C., Arbi, M., Pilz, G.-A., Pefani, D.-E., Lalioti, M.-E., Ninkovic, J., Götz, M., Lygerou, Z., and Taraviras, S. (2015). Mcidas and GemC1/Lynkeas are key regulators for the generation of multiciliated ependymal cells in the adult neurogenic niche. Development *142*, 3661–3674. https://doi.org/10.1242/dev.126342.

32. Tasic, B., Yao, Z., Graybuck, L.T., Smith, K.A., Nguyen, T.N., Bertagnolli, D., Goldy, J., Garren, E., Economo, M.N., Viswanathan, S., et al. (2018). Shared and distinct transcriptomic cell types across neocortical areas. Nature *563*, 72–78. https://doi.org/10.1038/s41586-018-0654-5.

33. Lewis, M., and Stracker, T.H. (2021). Transcriptional regulation of multiciliated cell differentiation. Semin. Cell Dev. Biol. *110*, 51–60. https://doi.org/10.1016/j.semcdb.2020.04.007.

34. La Manno, G., Siletti, K., Furlan, A., Gyllborg, D., Vinsland, E., Mossi Albiach, A., Mattsson Langseth, C., Khven, I., Lederer, A.R., Dratva, L.M., et al. (2021). Molecular architecture of the developing mouse brain. Nature *596*, 92–96. https://doi.org/10.1038/s41586-021-03775-x.

35. Di Bella, D.J., Habibi, E., Stickels, R.R., Scalia, G., Brown, J., Yadollahpour, P., Yang, S.M., Abbate, C., Biancalani, T., Macosko, E.Z., et al. (2021). Molecular logic of cellular diversification in the mouse cerebral cortex. Nature *595*, 554–559. https://doi.org/10.1038/s41586-021-03670-5.

36. Parichha, A., Suresh, V., Chatterjee, M., Kshirsagar, A., Ben-Reuven, L., Olender, T., Taketo, M.M., Radosevic, V., Bobic-Rasonja, M., Trnski, S., et al. (2022). Constitutive activation of canonical Wnt signaling disrupts choroid plexus epithelial fate. Nat. Commun. *13*, 633. https://doi.org/10.1038/s41467-021-27602-z.

37. Trousse, F., Poluch, S., Pierani, A., Dutriaux, A., Bock, H.H., Nagasawa, T., Verdier, J.M., and Rossel, M. (2015). CXCR7 receptor controls the maintenance of subpial positioning of cajal-retzius cells. Cereb. Cortex *25*, 3446–3457. https://doi.org/10.1093/cercor/bhu164.

38. Paredes, M.F., Li, G., Berger, O., Baraban, S.C., and Pleasure, S.J. (2006). Stromal-derived factor-1 (CXCL12) regulates laminar position of Cajal-Retzius cells in normal and dysplastic brains. J. Neurosci. *26*, 9404–9412. https://doi.org/10.1523/JNEUROSCI.2575-06.2006.

39. Borrell, V., and Marín, O. (2006). Meninges control tangential migration of hem-derived Cajal-Retzius cells via CXCL12/CXCR4 signaling. Nat. Neurosci. *9*, 1284–1293. https://doi.org/10.1038/nn1764.

40. Villar-Cerviño, V., Molano-Mazón, M., Catchpole, T., Valdeolmillos, M., Henkemeyer, M., Martínez, L.M., Borrell, V., and Marín, O. (2013). Contact repulsion controls the dispersion and final distribution of cajal-retzius cells. Neuron *77*, 457–471. https://doi.org/10.1016/j.neuron.2012.11.023.

41. Meyer, G., Cabrera Socorro, A., Perez Garcia, C.G., Martinez Millan, L., Walker, N., and Caput, D. (2004). Developmental roles of p73 in cajal-retzius cells and cortical patterning. J. Neurosci. *24*, 9878–9887. https://doi.org/10.1523/JNEUROSCI.3060-04.2004.

42. Yang, A., Walker, N., Bronson, R., Kaghad, M., Oosterwegel, M., Bonnin, J., Vagner, C., Bonnet, H., Dikkes, P., Sharpe, A.A., et al. (2000). p73-deficient mice have neurological, pheromonal and inflammatory defects but lack spontaneous tumours. Nature *404*, 99–103. https://doi.org/10.1038/35003607.

43. Pozniak, C.D., Radinovic, S., Yang, A., McKeon, F., Kaplan, D.R., and Miller, F.D. (2000). An anti-apoptotic role for the p53 family member, p73, during developmental neuron death. Science *289*, 304–306. https://doi.org/10.1126/science.289.5477.304.

44. Funk, M.C., Bera, A.N., Menchen, T., Kuales, G., Thriene, K., Lienkamp, S.S., Dengjel, J., Omran, H., Frank, M., and Arnold, S.J. (2015). Cyclin O (Ccno) functions during deuterosome-mediated centriole amplification of multiciliated cells. EMBO J. *34*, 1078–1089. https://doi.org/10.15252/embj.201490805.

45. Terré, B., Lewis, M., Gil-Gómez, G., Han, Z., Lu, H., Aguilera, M., Prats, N., Roy, S., Zhao, H., and Stracker, T.H. (2019). Defects in efferent duct multiciliogenesis underlie male infertility in GEMC1-, MCIDAS- or CCNO-deficient mice. Development *146*, dev162628. https://doi.org/10.1242/dev.162628.

46. Núnez-Ollé, M., Jung, C., Terré, B., Balsiger, N.A., Plata, C., Roset, R., Pardo-Pastor, C., Garrido, M., Rojas, S., Alameda, F., et al. (2017). Constitutive cyclin O deficiency results in penetrant hydrocephalus, impaired growth and infertility. Oncotarget *8*, 99261–99273. https://doi.org/10.18632/oncotarget.21818.

47. Zhao, H., Zhu, L., Zhu, Y., Cao, J., Li, S., Huang, Q., Xu, T., Huang, X., Yan, X., and Zhu, X. (2013). The Cep63 paralogue Deup1 enables massive de novo centriole biogenesis for vertebrate multiciliogenesis. Nat. Cell Biol. *15*, 1434–1444. https://doi.org/10.1038/ncb2880.

48. Mercey, O., Levine, M.S., LoMastro, G.M., Rostaing, P., Brotslaw, E., Gomez, V., Kumar, A., Spassky, N., Mitchell, B.J., Meunier, A., et al. (2019). Massive centriole production can occur in the absence of deuterosomes in multiciliated cells. Nat. Cell Biol. *21*, 1544–1552. https://doi.org/10.1038/s41556-019-0427-x.

49. Ortiz-Álvarez, G., Daclin, M., Shihavuddin, A., Lansade, P., Fortoul, A., Faucourt, M., Clavreul, S., Lalioti, M.-E., Taraviras, S., Hippenmeyer, S., et al. (2019). Adult neural stem cells and multiciliated ependymal cells share a common lineage regulated by the geminin family members. Neuron *102*, 159–172.e7. https://doi.org/10.1016/j.neuron.2019.01.051.

50. Meyer, G., González-Arnay, E., Moll, U., Nemajerova, A., Tissir, F., and González-Gómez, M. (2019). Cajal-Retzius neurons are required for the development of the human hippocampal fissure. J. Anat. *235*, 569–589. https://doi.org/10.1111/joa.12947.

51. Meyer, G. (2010). Building a human cortex: the evolutionary differentiation of Cajal-Retzius cells and the cortical hem. J. Anat. *217*, 334–343. https://doi.org/10.1111/j.1469-7580.2010.01266.x.

52. Roy, A., Gonzalez-Gomez, M., Pierani, A., Meyer, G., and Tole, S. (2014). Lhx2 regulates the development of the forebrain hem system. Cereb. Cortex *24*, 1361–1372. https://doi.org/10.1093/cercor/bhs421.

53. Subramanian, L., and Tole, S. (2009). Mechanisms underlying the specification, positional regulation, and function of the cortical hem. Cereb. Cortex *19*. i90–i95. https://doi.org/10.1093/cercor/bhp031.

54. Imayoshi, I., Shimogori, T., Ohtsuka, T., and Kageyama, R. (2008). Hes genes and neurogenin regulate non-neural versus neural fate specification in the dorsal telencephalic midline. Development *135*, 2531–2541. https://doi.org/10.1242/dev.021535.

55. Guo, Q., and Li, J.Y.H. (2019). Defining developmental diversification of diencephalon neurons through single-cell gene expression profiling. Development *146*, dev174284. https://doi.org/10.1242/dev.174284.

56. Godbole, G., Shetty, A.S., Roy, A., D'Souza, L., Chen, B., Miyoshi, G., Fishell, G., and Tole, S. (2018). Hierarchical genetic interactions between FOXG1 and LHX2 regulate the formation of the cortical hem in the developing telencephalon. Development *145*, 591–604. https://doi.org/10.1242/dev.154583.

57. Vyas, A., Saha, B., Lai, E., and Tole, S. (2003). Paleocortex is specified in mice in which dorsal telencephalic patterning is severely disrupted. J. Comp. Neurol. *466*, 545–553. https://doi.org/10.1002/cne.10900.

58. Muzio, L., and Mallamaci, A. (2005). Foxg1 confines Cajal-Retzius neuronogenesis and hippocampal morphogenesis to the dorsomedial pallium. J. Neurosci. *25*, 4435–4441. https://doi.org/10.1523/JNEUROSCI.4804-04.2005.

59. Mangale, V.S., Hirokawa, K.E., Satyaki, P.R.V., Gokulchandran, N., Chikbire, S., Subramanian, L., Shetty, A.S., Martynoga, B., Paul, J., Mai, M.V., et al. (2008). Lhx2 selector activity specifies cortical identity and suppresses hippocampal organizer fate. Science *319*, 304–309. https://doi.org/10.1126/science.1151695.

60. Ratz, M., von Berlin, L., Larsson, L., Martin, M., Westholm, J.O., La Manno, G., Lundeberg, J., and Frisén, J. (2022). Clonal relations in the mouse brain revealed by single-cell and spatial transcriptomics. Nat. Neurosci. *25*, 285–294. https://doi.org/10.1038/s41593-022-01011-x.

61. Fame, R.M., Cortés-Campos, C., and Sive, H.L. (2020). Brain ventricular system and cerebrospinal fluid development and function: light at the end of the tube: A primer with latest insights. BioEssays *42*, e1900186. https://doi.org/10.1002/bies.201900186.

62. Bill, B.R., and Korzh, V. (2014). Choroid plexus in developmental and evolutionary perspective. Front. Neurosci. *8*, 363. https://doi.org/10.3389/fnins.2014.00363.

63. Defosset, A., Merlat, D., Poidevin, L., Nevers, Y., Kress, A., Poch, O., and Lecompte, O. (2021). Novel approach combining transcriptional and evolutionary signatures to identify new multiciliation genes. Genes (Basel) *12*, 1452. https://doi.org/10.3390/genes12091452.

64. Cabrera-Socorro, A., Hernandez-Acosta, N.C., Gonzalez-Gomez, M., and Meyer, G. (2007). Comparative aspects of p73 and Reelin expression in Cajal-Retzius cells and the cortical hem in lizard, mouse and human. Brain Res. *1132*, 59–70. https://doi.org/10.1016/j.brainres.2006.11.015.

65. Tissir, F., Lambert De Rouvroit, C., Sire, J.-Y., Meyer, G., and Goffinet, A.M. (2003). Reelin expression during embryonic brain development in Crocodylus niloticus. J. Comp. Neurol. *457*, 250–262. https://doi.org/10.1002/cne.10573.

66. Meunier, A., and Azimzadeh, J. (2016). Multiciliated cells in animals. Cold Spring Harb. Perspect. Biol. *8*, a028233. https://doi.org/10.1101/cshperspect.a028233.

67. Amelio, I., Panatta, E., Niklison-Chirou, M.V., Steinert, J.R., Agostini, M., Morone, N., Knight, R.A., and Melino, G. (2020). The C terminus of p73 is essential for hippocampal development. Proc. Natl. Acad. Sci. USA *117*, 15694–15701. https://doi.org/10.1073/pnas.2000917117.

68. Medina-Bolívar, C., González-Arnay, E., Talos, F., González-Gómez, M., Moll, U.M., and Meyer, G. (2014). Cortical hypoplasia and ventriculomegaly of p73-deficient mice: developmental and adult analysis. J. Comp. Neurol. *522*, 2663–2679. https://doi.org/10.1002/cne.23556.

69. Gonzalez-Cano, L., Fuertes-Alvarez, S., Robledinos-Anton, N., Bizy, A., Villena-Cortes, A., Fariñas, I., Marques, M.M., and Marin, M.C. (2016). p73 is required for ependymal cell maturation and neurogenic SVZ cytoarchitecture. Dev. Neurobiol. *76*, 730–747. https://doi.org/10.1002/dneu.22356.

70. Fuertes-Alvarez, S., Maeso-Alonso, L., Villoch-Fernandez, J., Wildung, M., Martin-Lopez, M., Marshall, C., Villena-Cortes, A.J., Diez-Prieto, I., Pietenpol, J.A., Tissir, F., et al. (2018). p73 regulates ependymal planar cell polarity by modulating actin and microtubule cytoskeleton. Cell Death Dis. *9*, 1183. https://doi.org/10.1038/s41419-018-1205-6.

71. Nemajerova, A., Kramer, D., Siller, S.S., Herr, C., Shomroni, O., Pena, T., Gallinas Suazo, C., Glaser, K., Wildung, M., Steffen, H., et al. (2016). TAp73 is a central transcriptional regulator of airway multiciliogenesis. Genes Dev. *30*, 1300–1312. https://doi.org/10.1101/gad.279836.116.

72. Ledonne, F., Orduz, D., Mercier, J., Vigier, L., Grove, E.A., Tissir, F., Angulo, M.C., Pierani, A., and Coppola, E. (2016). Targeted inactivation of Bax reveals a subtype-specific mechanism of cajal-retzius neuron death in the postnatal cerebral cortex. Cell Rep. *17*, 3133–3141. https://doi.org/10.1016/j.celrep.2016.11.074.

73. Chowdhury, T.G., Jimenez, J.C., Bomar, J.M., Cruz-Martin, A., Cantle, J.P., and Portera-Cailliau, C. (2010). Fate of cajal-retzius neurons in the postnatal mouse neocortex. Front. Neuroanat. *4*, 10. https://doi.org/10.3389/neuro.05.010.2010.

74. Derer, P., and Derer, M. (1990). Cajal-retzius cell ontogenesis and death in mouse brain visualized with horseradish peroxidase and electron microscopy. Neuroscience *36*, 839–856. https://doi.org/10.1016/0306-4522(90)90027-2.

75. Causeret, F., Coppola, E., and Pierani, A. (2018). Cortical developmental death: selected to survive or fated to die. Curr. Opin. Neurobiol. *53*, 35–42. https://doi.org/10.1016/j.conb.2018.04.022.

76. Becker-Heck, A., Zohn, I.E., Okabe, N., Pollock, A., Lenhart, K.B., Sullivan-Brown, J., McSheene, J., Loges, N.T., Olbrich, H., Haeffner, K., et al. (2011). The coiled-coil domain containing protein CCDC40 is essential for motile cilia function and left-right axis formation. Nat. Genet. *43*, 79–84. https://doi.org/10.1038/ng.727.

77. Muthusamy, N., Vijayakumar, A., Cheng, G., and Ghashghaei, H.T. (2014). A Knock-in Foxj1 CreERT2::GFP mouse for recombination in epithelial cells with motile cilia. Genesis *52*, 350–358. https://doi.org/10.1002/dvg.22753.

78. Lallemand, Y., Luria, V., Haffner-Krausz, R., and Lonai, P. (1998). Maternally expressed PGK-Cre transgene as a tool for early and uniform activation of the Cre site-specific recombinase. Transgen. Res. *7*, 105–112. https://doi.org/10.1023/a:1008868325009.

79. Gorski, J.A., Talley, T., Qiu, M., Puelles, L., Rubenstein, J.L.R.R., and Jones, K.R. (2002). Cortical excitatory neurons and glia, but not GABAergic neurons, are produced in the Emx1-expressing lineage. J. Neurosci. *22*, 6309–6314. https://doi.org/10.1523/JNEUROSCI.22-15-06309.2002.

80. Berger, J., Eckert, S., Scardigli, R., Guillemot, F., Gruss, P., and Stoykova, A. (2004). E1-Ngn2/Cre is a new line for regional activation of Cre recombinase in the developing CNS. Genesis *40*, 195–199. https://doi.org/10.1002/gene.20081.

81. Srinivas, S., Watanabe, T., Lin, C.S., William, C.M., Tanabe, Y., Jessell, T.M., and Costantini, F. (2001). Cre reporter strains produced by targeted insertion of EYFP and ECFP into the ROSA26 locus. BMC Dev. Biol. *1*, 4. https://doi.org/10.1186/1471-213x-1-4.

82. Madisen, L., Zwingman, T.A., Sunkin, S.M., Oh, S.W., Zariwala, H.A., Gu, H., Ng, L.L., Palmiter, R.D., Hawrylycz, M.J., Jones, A.R., et al. (2010). A robust and high-throughput Cre reporting and characterization system for the whole mouse brain. Nat. Neurosci. *13*, 133–140. https://doi.org/10.1038/nn.2467.

83. Tao, W., and Lai, E. (1992). Telencephalon-restricted expression of BF-1, a new member of the HNF-3/fork head gene family, in the developing rat brain. Neuron *8*, 957–966. https://doi.org/10.1016/0896-6273(92)90210-5.

84. Schiffmann, S.N., Bernier, B., and Goffinet, A.M. (1997). Reelin mRNA expression during mouse brain development. Eur. J. Neurosci. *9*, 1055–1071. https://doi.org/10.1111/j.1460-9568.1997.tb01456.x.

85. Grove, E.A., Tole, S., Limon, J., Yip, L., and Ragsdale, C.W. (1998). The hem of the embryonic cerebral cortex is defined by the expression of multiple Wnt genes and is compromised in Gli3-deficient mice. Development *125*, 2315–2325. https://doi.org/10.1242/dev.125.12.2315.

86. Hao, Y., Hao, S., Andersen-Nissen, E., Mauck, W.M., Zheng, S., Butler, A., Lee, M.J., Wilk, A.J., Darby, C., Zager, M., et al. (2021). Integrated analysis of multimodal single-cell data. Cell *184*, 3573–3587.e29. https://doi.org/10.1016/j.cell.2021.04.048.

87. Wolock, S.L., Lopez, R., and Klein, A.M. (2019). Scrublet: computational identification of cell doublets in single-cell transcriptomic data. Cell Syst. *8*, 281–291.e9. https://doi.org/10.1016/j.cels.2018.11.005.

88. Weinreb, C., Wolock, S., and Klein, A.M. (2018). SPRING: a kinetic interface for visualizing high dimensional single-cell expression data. Bioinformatics *34*, 1246–1248. https://doi.org/10.1093/bioinformatics/btx792.

89. Dey, K.K., Hsiao, C.J., and Stephens, M. (2017). Visualizing the structure of RNA-seq expression data using grade of membership models. PLoS Genet. *13*, e1006599. https://doi.org/10.1371/journal.pgen.1006599.

90. Carbonetto, P., Sarkar, A., Wang, Z., and Stephens, M. (2021). Non-negative matrix factorization algorithms greatly improve topic model fits. arXiv. https://doi.org/10.48550/arXiv.2105.13440.

91. Tasic, B., Menon, V., Nguyen, T.N., Kim, T.K., Jarsky, T., Yao, Z., Levi, B., Gray, L.T., Sorensen, S.A., Dolbeare, T., et al. (2016). Adult mouse cortical cell taxonomy revealed by single cell transcriptomics. Nat. Neurosci. *19*, 335–346. https://doi.org/10.1038/nn.4216.

92. Herman, J.S., Sagar, and Grün, D. (2018). FateID infers cell fate bias in multipotent progenitors from single-cell RNA-seq data. Nat. Methods *15*, 379–386. https://doi.org/10.1038/nmeth.4662.

93. Schwabe, D., Formichetti, S., Junker, J.P., Falcke, M., and Rajewsky, N. (2020). The transcriptome dynamics of single cells during the cell cycle. Mol. Syst. Biol. *16*, e9946. https://doi.org/10.15252/msb.20209946.

94. Trapnell, C., Cacchiarelli, D., Grimsby, J., Pokharel, P., Li, S., Morse, M., Lennon, N.J., Livak, K.J., Mikkelsen, T.S., and Rinn, J.L. (2014). The dynamics and regulators of cell fate decisions are revealed by pseudotemporal ordering of single cells. Nat. Biotechnol. *32*, 381–386. https://doi.org/10.1038/nbt.2859.

95. Kolberg, L., Raudvere, U., Kuzmin, I., Vilo, J., and Peterson, H. (2020). gprofiler2 – an R package for gene list functional enrichment analysis and namespace conversion toolset g:profiler. F1000Res *9*, ELIXIR-709. https://doi.org/10.12688/f1000research.24956.2.

96. Arai, Y., Cwetsch, A.W., Coppola, E., Cipriani, S., Nishihara, H., Kanki, H., Saillour, Y., Freret-Hodara, B., Dutriaux, A., Okada, N., et al. (2019). Evolutionary gain of Dbx1 expression drives subplate identity in the cerebral cortex. Cell Rep. *29*, 645–658.e5. https://doi.org/10.1016/j.celrep.2019.09.007.

97. Susaki, E.A., Tainaka, K., Perrin, D., Yukinaga, H., Kuno, A., and Ueda, H.R. (2015). Advanced CUBIC protocols for whole-brain and whole-body clearing and imaging. Nat. Protoc. *10*, 1709–1727. https://doi.org/10.1038/nprot.2015.085.

98. Schaeren-Wiemers, N., and Gerfin-Moser, A. (1993). A single protocol to detect transcripts of various types and expression levels in neural tissue and cultured cells: in situ hybridization using digoxigenin-labelled cRNA probes. Histochemistry *100*, 431–440. https://doi.org/10.1007/BF00267823.

99. Causeret, F., Ensini, M., Teissier, A., Kessaris, N., Richardson, W.D., Lucas de Couville, T.L., and Pierani, A. (2011). Dbx1-expressing cells are necessary for the survival of the mammalian anterior neural and craniofacial structures. PLoS One *6*. e19367. https://doi.org/10.1371/journal.pone.0019367.

Please cite this article in press as: Moreau et al., Repurposing of the multiciliation gene regulatory network in fate specification of Cajal-Retzius neurons, Developmental Cell (2023), https://doi.org/10.1016/j.devcel.2023.05.011

STAR★METHODS

KEY RESOURCES TABLE

REAGENT or RESOURCE	SOURCE	IDENTIFIER
Antibodies		
Chicken Polyclonal Anti GFP	Aves Labs	Cat# GFP-1020; RRID: AB_10000240
Rabbit Polyclonal Anti dsRed	Clontech Laboratories	Cat# 632496; RRID: AB_10013483
Mouse monoclonal Anti Ebf3	Abnova	Cat # H00253738-M05; RRID: AB_565597
Mouse monoclonal Anti Reln (G10)	Millipore	Cat# MAB5364; Clone G10; RRID: AB_2179313
Rabbit monoclonal Anti Trp73	Cell signaling	Cat# 14620; Clone D3G10; RRID: AB_2798542
Rabbit monoclonal Anti Tbr2	Abcam	Cat# ab216870
Rat Monoclonal Antibody Anti Tbr2/Eomes	Thermo Fisher Scientific	Cat# 14-4875-82; RRID: AB_11042577
Rabbit polyclonal Anti Foxg1	Abcam	Cat# ab18259; RRID: AB_732415
Rabbit monoclonal Anti Caspase-3	Cell Signaling	Cat# 9664; RRID: AB_2070042
Mouse monoclonal Anti FOP	Abnova	Cat# H00011116-M01; Clone: 2B1; RRID: AB_463883
Rabbit monoclonal Anti Arl13b	Gift from Prof. Tamara Caspary (Emory University)	N/A
Rat monoclonal Anti p21	Abcam	Cat# ab107099; RRID: AB_10891759
Goat polyclonal Anti Reln	R&D Systems	Cat# AF3820; RRID: AB_2253745
Donkey polyclonal Anti chick Alexa-488	Jackson ImmunoResearch	Cat# 703-545-155; RRID: AB_2340375
Donkey polyclonal Anti mouse Cy3	Jackson ImmunoResearch	Cat# 715-165-151; RRID: AB_2315777
Donkey polyclonal Anti mouse Cy5	Jackson ImmunoResearch	Cat# 715-175-151; RRID: AB_2340820
Donkey polyclonal Anti rabbit Cy3	Jackson ImmunoResearch	Cat# 711-165-152; RRID: AB_2307443
Donkey polyclonal Anti rabbit Cy5	Jackson ImmunoResearch	Cat# 711-175-152; RRID: AB_2340607
Donkey polyclonal Anti rabbit DyLight 405	Jackson ImmunoResearch	Cat# 711-475-152; RRID: AB_2340616
Donkey polyclonal Anti rabbit Alexa-488	Jackson ImmunoResearch	Cat# 711-545-152,;RRID: AB_2313584
Sheep polyclonal Anti-Digoxigenin-AP, Fab fragments antibody	Roche	Cat# 11093274910; RRID: AB_2734716
Sheep polyclonal Anti-Digoxigenin Fab fragments Antibody, POD Conjugated	Roche	Cat# 11207733910; RRID: AB_514500
Bacterial and virus strains		
One Shot™ TOP10 competent E. coli	Invitrogen	Cat# C404010
Chemicals, peptides, and recombinant proteins		
DIG-RNA labeling kit	Roche	Cat# 11277073910
Phusion DNA polymerase	Thermo Scientific	Cat # F530S
XhoI	Thermo Scientific	Cat# FD0694
SalI	Thermo Scientific	Cat# FD0644
T4 DNA ligase	Thermo Scientific	Cat# EL0014
DAPI (4', 6-diamidino-2-phenylindole)	Thermo Scientific	Cat# D1306
DNase I	New England BioLabs	Cat# M0303S
T7 RNA Polymerase	New England BioLabs	Cat# M0251S
RNasin® Ribonuclease Inhibitors	Promega	Cat# N2511
4-Nitro blue tetrazolium chloride, solution	Roche	Cat# 11383213001
4-toluidine salt (BCIP)	Roche	Cat# 11383221001
TSA Plus Cyanine 3 Kit	PerkinElmer	Cat# NEL744001KT
TO-PRO-3	Invitrogen	Cat# T3605
(Ethylenedinitrilo)tetra-2-propanol, Quadrol®	Sigma-Aldrich	Cat# 122262
Critical commercial assays		
Chromium Next GEM Single Cell 3' Kit v3.1	10X Genomics	PN-1000269

(*Continued on next page*)

Please cite this article in press as: Moreau et al., Repurposing of the multiciliation gene regulatory network in fate specification of Cajal-Retzius neurons, Developmental Cell (2023), https://doi.org/10.1016/j.devcel.2023.05.011

Continued

REAGENT or RESOURCE	SOURCE	IDENTIFIER
Chromium Single Cell 3' GEM, Library & Gel Bead Kit v3	10X Genomics	PN-1000092
Neural Tissue Dissociation Kit (P)	Miltenyi Biotec	Cat # 130-092-628
Nucleobond Xtra Maxi EF dnkit	Macherey-Nagel	Cat # 740424.10
Apoptag Peroxidase in situ Apoptosis Detection kit	Millipore	Cat# S7100
Deposited data		
Raw and analyzed single-cell sequencing data	This paper	GEO: GSE220237
R codes for analysis	This paper	https://doi.org/10.5281/zenodo.7664134 and https://fcauseret.github.io/hemCR
Experimental models: Organisms/strains		
C57BL/6J	Janvier Labs	RRID: IMSR_JAX:000664
Gmnc -/- (Gmnc tm1.1Strc)	Terré et al.[29]	N/A
Trp73 -/- (Trp73 tm1Fmc)	Yang et al.[42]	RRID: MGI:5289954
Ccdc67 -/- (Deup1 tm1.1(KOMP)Vlcg)	Mercey et al.[48]	N/A
Ccno -/- (Ccno tm1.1(KOMP)Vlcg)	Núnez-Ollé et al.[46]	N/A
Ccdc40 -/- (Ccdc40 Inks)	Becker-Heck et al.[76]	RRID: MGI:4939592
Foxj1 CreERT2 (Foxj1 tm1.1(cre/ERT2/GFP)Htg)	Muthusamy et al.[77]	RRID: IMSR_JAX:027012
PGK Cre (Tg(Pgk1-cre)1Lni)	Lallemand et al.[78]	N/A
Emx1 Cre (Emx1 tm1(cre)Krj)	Gorsky et al.[79]	N/A
ΔNp73 Cre (Trp73 tm1(cre)Agof)	Tissir et al.[21]	N/A
Wnt3a Cre (Wnt3a tm1(cre)Eag)	Yoshida et al.[19]	N/A
E1-Ngn2 Cre (Tg(Neurog2-cre/GFP)1Stoy)	Berger et al.[80]	N/A
Rosa26 YFP (Gt(ROSA)26Sor tm1(EYFP)Cos)	Srinivas et al.[81]	N/A
Rosa26 tdTomato (Gt(ROSA)26Sor tm9(CAG-tdTomato)Hze)	Madisen et al.[82]	N/A
Oligonucleotides		
See Table S1	This paper	N/A
Recombinant DNA		
pCAGGs-Lox-STOP-Lox-IRES-GFP (pCAG-LSL)	This paper	N/A
pCAGGs-Lox-STOP-Lox-Gmnc-IRES-GFP (pCAG-LSL-Gmnc)	This paper	N/A
pCAGGS-mcherry	Addgene	Cat# 41583; RRID: Addgene_41583
Foxg1 ISH probe plasmid	Tao et al.[83]	N/A
Reln ISH probe plasmid	Schiffmann et al.[84]	N/A
Trp73 ISH probe plasmid	Takiguchi-Hayashi et al.[16]	N/A
Wnt3a ISH probe plasmid	Grove et al.[85]	N/A
Software and algorithms		
Cell Ranger v3.1.0	10X Genomics	https://support.10xgenomics.com/single-cell-gene-expression/software/overview/welcome
Cell Ranger v6.0.0	10X Genomics	https://support.10xgenomics.com/single-cell-gene-expression/software/overview/welcome
Seurat v4.0.5	Hao et al.[86]	https://github.com/satijalab/seurat/releases/tag/v4.0.5
Scrublet v0.2.2	Wolock et al.[87]	https://github.com/swolock/scrublet
SPRING tool	Weinreb et al.[88]	https://github.com/AllonKleinLab/SPRING_dev
fastTopic (v.5.59)	Dey et al.,[89] Carbonetto et al.[90]	https://github.com/stephenslab/fastTopics
scrattch.hicat v0.0.16	Tasic et al.[91]	https://github.com/AllenInstitute/scrattch.hicat
FateID v0.1.9	Herman et al.[92]	https://github.com/dgrun/FateID
Revelio v0.1.0	Schwabe et al.[93]	https://github.com/danielschw188/Revelio

(*Continued on next page*)

Please cite this article in press as: Moreau et al., Repurposing of the multiciliation gene regulatory network in fate specification of Cajal-Retzius neurons, Developmental Cell (2023), https://doi.org/10.1016/j.devcel.2023.05.011

Continued

REAGENT or RESOURCE	SOURCE	IDENTIFIER
Monocle v2.22.0	Trapnell et al.[94]	https://github.com/cole-trapnell-lab/monocle-release
Gprofiler2 v2_0.2.1	Kolberg et al.[95]	https://cran.r-project.org/web/packages/gprofiler2/index.html
Other		
MACS® SmartStrainers 30 μm	Miltenyi Biotec	130-098-458
pluriStrainer Mini 10 μm	pluriSelect	43-10010-40
NEPA21 electroporator	Nepagene	N/A

RESOURCE AVAILABILITY

Lead contact

Further information and requests for resources and reagents should be directed to and will be fulfilled by the lead contact, Frédéric Causeret (frederic.causeret@inserm.fr).

Materials availability

Plasmids generated in this study are available upon request.

Data and code availability

Raw scRNAseq reads and processed count matrix are available from the Gene Expression Omnibus under accession number GEO: GSE220237. R codes have been deposited at Zenodo (DOI indicated in key resources table) and are also available, together with metadata, at https://fcauseret.github.io/hemCR.

EXPERIMENTAL MODEL AND STUDY PARTICIPANT DETAILS

Mouse strains

The following mouse lines were used and maintained on a C57BL/6J background: *Gmnc*$^{-/-}$ (*Gmnc*$^{tm1.1Strc}$),[29] *Trp73*$^{-/-}$ (*Trp73*^{tm1Fmc}),[42] *Ccdc67*$^{-/-}$ (*Deup1*$^{tm1.1(KOMP)Vlcg}$),[48] *Ccno*$^{-/-}$ (*Ccno*$^{tm1.1(KOMP)Vlcg}$),[46] *Ccdc40*$^{-/-}$ (*Ccdc40*^{lnks}),[76] *Foxj1*^{CreERT2} (*Foxj1*$^{tm1.1(cre/ERT2/GFP)Htg}$),[77] *PGK*^{Cre} (*Tg(Pgk1-cre)1Lni*),[78] *Emx1*^{Cre} (*Emx1*$^{tm1(cre)Krj}$),[79] *ΔNp73*^{Cre} (*Trp73*$^{tm1(cre)Agof}$),[21] *Wnt3a*^{Cre} (*Wnt3a*$^{tm1(cre)Eag}$),[19] *E1-Ngn2*^{Cre} (*Tg(Neurog2-cre/GFP)1Stoy*),[80] *Rosa26*^{YFP} (*Gt(ROSA)26Sor*$^{tm1(EYFP)Cos}$)[81] and *Rosa26*^{tdTomato} (*Gt(ROSA)26Sor*$^{tm9(CAG-tdTomato)Hze}$).[82] All animals were housed in individually ventilated cages containing tube shelters and nesting material, maintained at 20°C and 50% humidity, under a 12h light/dark cycle, with food and water *ad libitum*. They were handled in strict accordance with good animal practice, as defined by the national animal welfare bodies, and all mouse work was approved by either the French Ministry of Higher Education, Research and Innovation as well as the Animal Experimentation Ethical Committee of Université Paris Cité (CEEA-34, licence numbers: 2020012318201928 and 2018020717269338), or the institutional ethics committee from Universidad de Leon and Junta de Castilla y Leon (approval OEBAULE-018-2017 and OEBA-ULE-018-2021).

METHOD DETAILS

scRNAseq

Six *PGK*^{Cre}; *Rosa26*^{YFP} E11.5 embryos originating from two distinct litters and four *Wnt3a*^{Cre}; *Rosa26*^{tdTomato} E12.5 embryos obtained from the same litter were collected in HBSS on ice to generate the wild-type reference dataset. *Gmnc*$^{-/-}$ cells were obtained from four pooled E12.5 mutant embryos collected from two distinct litters. For each dataset, a region spanning the dorsal pallial midline (see Figure 1A) was dissected on both hemispheres and dissociated using the Neural Tissue Dissociation Kit (P) (Miltenyi Biotec) on the gentleMACS Octo Dissociator following the manufacturer's instructions. Remaining clumps of cells and debris were removed via two rounds of centrifugation for 3 min at 200 g followed by filtration through 30 μm cell strainers (Miltenyi Biotec). To ensure all remaining cells aggregates were dissociated, we finally pipetted the suspension through Gel Saver tips (QSP) and proceeded to a last filtration through a 10 μm cell strainer (pluriSelect). Cell viability and concentration were assessed using a MACSQuant flow cytometer (Miltenyi Biotec). Approximatively 20000 cells were used as input on the 10X Genomics Chromium Controller for a targeted cell recovery of 10000 cells per library. The entire procedure, from the sacrifice of the pregnant female until loading the controller, was achieved in 2h. For the wild-type dataset, two Single Cell 3′ Kit v3 libraries were produced and sequenced on a NovaSeq 6000 sequencer at a total depth of 800 million reads. For the mutant dataset, one Single Cell 3' Kit v3.1 library was produced and sequenced at a depth of 750 million reads. Raw sequencing reads were processed to counts matrix with Cell Ranger version 3.1.0 (wild-type) or 6.0.0 (KO) using default parameters and the mm10 mouse genome reference to which the sequenced of *YFP* and *tdTomato* were added. All statistical analyses were performed under R version 4.1.2.

Please cite this article in press as: Moreau et al., Repurposing of the multiciliation gene regulatory network in fate specification of Cajal-Retzius neurons, Developmental Cell (2023), https://doi.org/10.1016/j.devcel.2023.05.011

Cell filtering

Each library was processed independently to extract high-quality cells from the raw count matrix. Cells were filtered based on the percentage of UMI associated with mitochondrial transcripts and number of detected genes, to keep only those within a three median absolute deviation (MAD) around the population median for these metrics. We further excluded cells having a UMI number above 3 MADs of the population median. Potential doublets were removed using Scrublet.[87] Dimensionality reduction was performed using the SPRING tool[88] as we found it outperforms UMAP for its ability to align cells along a differentiation axis and capture the continuity of cell states in our dataset (compare Figures 1B and S1D). To combine wild-type and mutant datasets into the same reduced space, we projected the mutant cells onto control cells using the dedicated algorithm implemented in SPRING. Counts values were library size normalised and scaled using Seurat (v 4.0.5).[86]

Broad clustering and cell type annotation

For each dataset, we first apply coarse Louvain clustering and use known marker gene to identify the major classes of radial glia progenitor, and neuronal cells. Wild-type neuronal cells were extracted and separated into two lineages during a second round of Louvain clustering. Belonging to CRs or pallial neurons lineages was readily identified based on the exclusive expression of the transcription factors *Trp73* or *Foxg1*.

To further resolve the diversity among wild-type progenitors and ChP populations, we first performed topic modeling using fastTopic (v.5.59).[89,90] Then, progenitors were grouped into 6 clusters by applying partition around medoids to the loading of the 6 topics which best captured progenitor domain identities. Finally, top marker genes for each inferred cluster were used to validate their annotation by mapping their position on tissue using ISH.

In order to annotate the mutant dataset, we first extracted progenitor cells and transferred the wild-type ISH-validated cluster annotation using SeuratV4 functions "FindTransferAnchors" and "TransferData". We then extracted neuronal cells and identified the most mature cells after fitting a principal curve to their SPRING coordinates. These cells were then subject to iterative clustering using scrattch.hicat (v0.0.16)[91] to identify the 3 population corresponding respectively to the hem- and ThE-derived CRs and pallial neurons. Finally, annotation of the intermediate states cells was predicted using FateID (v0.1.9)[92] seeded with the 3 clusters of mature neurones found in this dataset.

The multiciliation score was computed based on the combined expression of 28 mutliciliation genes described by Lewis et al.[33] using the Seurat function AddModuleScore.

Trajectories

For each neuronal differentiation trajectory, a pseudotime axis was fitted in two steps. First, we extracted apical progenitors belonging to the cortical hem or medial pallium cluster. These progenitors were then aligned along their cell cycle axis, from G1 to M phase using the Revelio package (v0.1.0).[93] In parallel, a principal curve was fitted on the SPRING coordinates of the two neuronal lineages cells to capture the pan-neuronal differentiation axis. In a second step, the two ordering of progenitors and neurons were concatenated into the same pseudotime axis, with progenitors arbitrarily allocated to the first 1/3 of the full trajectory. With this approach, differentiation trajectories therefore start at the G1 phase in apical progenitors.

Differentially expressed genes along pseudotime between the two trajectories were identified using the likelihood ratio test implemented in the function 'differentialGeneTest' of the package Monocle (v2.22.0).[94] Trajectory-specific enrichment was determined by computing the area between the two curves as performed by Monocle. Genes with similar smoothed trends were grouped into 6 clusters using partition around medoids. Finally, gene list functional enrichment analysis was performed using gprofiler2 (v2_0.2.1).

ScRNAseq atlas analysis

Developing mouse brain atlas[34] gene expression levels and cell metadata were retrieved from http://mousebrain.org/. We used LoomR 0.2.1.9000 (https://github.com/mojaveazure/loomR) to extract "Forebrain" and "Head" cells annotated as "Neuron", "Neuroblast", "Radial glia" and "Choroid plexus" from time points E10.0 to E18.0. A final subset of 101,567 cells was retained. The developing mouse cortex atlas[35] dataset was retrieved from the Single Cell Portal (https://singlecell.broadinstitute.org/single_cell/study/SCP1290/molecular-logic-of-cellular-diversification-in-the-mammalian-cerebral-cortex). For both datasets, raw count values were normalized to the library size and scaled using Seurat (version 4.0.5). UMAP dimensionality reduction was performed using the first 25 principal components for the *La Manno* et al. dataset, whereas UMAP coordinates of the *Di Bella* et al. atlas were obtained from the Single Cell Portal.

Cloning

Gmnc coding sequence (CDS) was inserted into a pCAGGs-Lox-STOP-Lox-IRES-GFP (pCAG-LSL) as follows. First, *Gmnc* CDS was amplified by PCRs from a pCAGGS-Gmnc plasmid[31] using Phusion DNA polymerase (Thermo Scientific F530S) and primers carrying XhoI or SalI restriction sites. Then, DNA digestion of the pCAG-LSL and *Gmnc* cDNA was performed with XhoI (Thermo Scientific FD0694) and SalI (Thermo Scientific FD0644) and the *Gmnc* fragment inserted in the backbone by enzymatic ligation using T4 ligase (Thermo Scientific EL0014). Plasmid amplification was performed in One Shot™ TOP10 competent E. coli (Invitrogen C404010) and purification was achieved using an Nucleobond Xtra Maxi EF kit (Macherey-Nagel 740424.10). Plasmids were verified by restriction and sequencing to confirm the correct insertion.

Please cite this article in press as: Moreau et al., Repurposing of the multiciliation gene regulatory network in fate specification of Cajal-Retzius neurons, Developmental Cell (2023), https://doi.org/10.1016/j.devcel.2023.05.011

Electroporation

E12.5 or E13.5 pregnant females (wild-type or transgenic) were anaesthetised with Isoflurane (4% induction, 2% during the surgery) and subjected to abdominal incision to expose the uterine horns. A combination of pCAG-LSL-Gmnc-GFP and pCAGGs-mCherry[96] at a final concentration of 1 μg/μl and mixed with Fast Green was injected into the lateral ventricles of embryos with a glass capillary. A train of five pulses (30 V, 50 ms, 1Hz) was applied to injected embryos through the uterus using a NEPA21 electroporator (Nepagene). Uterine horns were repositioned into the abdominal cavity, and the abdominal wall and skin were sutured. Embryos were harvested 3days later.

Tissue processing

Embryos were staged, starting from midday of the vaginal plug considered as embryonic day 0.5 (E0.5). After collection and dissection in ice-cold PBS, embryos were immediately fixed by immersion in 4% paraformaldehyde, 0.12 M phosphate buffer (PB) (pH 7.4), at 4°C for 2 h for E11.5-E12.5 to 3 h for E13.5. Cryoprotection was achieved by overnight incubation in 10% sucrose, PB at 4°C, before embedding in 7.5% gelatine, 10% sucrose in PB, and freezing by immersion in isopentane cooled at −55°C. 20 μm coronal sections were obtained with a Leica CM3050 cryostat and collected on Superfrost Plus slides (Menzell-Glasser).

Tissue clearing

We performed whole head clearing according to the advanced CUBIC protocol.[97] Tissues were fixed with 4% paraformaldehyde in PBS, for 2h30 at 4°C, and washed 3 times in PBS 1X for 1 h. For the delipidation step, tissues were incubated in the Sca*l*eCUBIC-1 reagent at RT for 1 week followed by 6 washes in PBS 1X for 1h. After permeabilisation in PBS 0.2% Gelatin, 0.5% Triton-X100, tissues were incubated with primary antibodies for 1 week. Excess of antibodies were removed during 6 washes in PBS 1X for 1h. Secondary antibodies were incubated with TO-PRO-3 for 3 days. All steps were performed at RT with agitation. Brains were finally cleared in the aqueous solution of Sca*l*eCUBIC-2 reagent.

Immunostaining

Antibodies indicated in the key resources table were used at the following concentration: chick anti-GFP (1:1000), rabbit anti-Tomato (1:500), mouse anti-Ebf3 (1:1000), mouse anti-Reln (1:300), rabbit anti-Trp73 (1:250), rabbit anti-Tbr2 (1:300, used in Figure S4B), rat anti-Tbr2 (1:300, used in Figure S7A), rabbit anti-Foxg1 (1:1000), rabbit anti-Caspase 3 (1:400), mouse anti-FOP (1:500), rabbit anti-Arl13b (1:500), rat anti-p21 (1:200), donkey anti-chick Alexa-488 (1:1000), donkey anti-mouse Cy5 (1:500), donkey anti-rabbit Cy3 (1:700) and donkey anti-rabbit Cy5 (1:500). DAPI (1 μg/ml) was used for nuclear staining. Slides were mounted in Vectashield (Vector).

In situ hybridisation

For each gene of interest, a DNA fragment (typically 500-800 bp) was amplified by PCRs from an embryonic brain cDNA library using Phusion polymerase (Thermo) and primers indicated in Table S1. The promoter sequence of the T7 RNA polymerase (GGTAATACGACTCACTATAGGG) was added in 5′ of reverse primers. Alternatively, for mouse *Foxg1*,[83] *Reln*,[84] *Trp73*[16] and *Wnt3a*,[85] a plasmid containing part of the cDNA was linearised by enzymatic restriction. Antisense digoxigenin-labelled RNA probes were then obtained by *in vitro* transcription using T7, T3 or SP6 RNA polymerase (New England Biolabs) and digRNA labelling mix (Roche). ISH was carried out as previously described[98] using a hybridisation buffer composed of 50% formamide, 5×SSC, 1×Denhardt's, 10% dextran sulfate, 0.5 mg/ml yeast RNA and 0.25 mg/ml herring sperm DNA. Probes were detected using an anti-digoxigenin antibody coupled to alkaline phosphatase (Roche) and NBT/BCIP (Roche) as substrates. Slides were mounted in Mowiol. *Gmnc* fluorescent ISH was carried out as described above with the following modifications. Proteinase K treatment was replaced by permeabilisation with RIPA buffer. Slides were incubated 30 min in 2% H_2O_2 in ethanol to block endogenous peroxydase activity. The *Gmnc* probe was detected using a peroxidase-conjugated anti-digoxigenin antibody (Roche) and Cy3-tyramide (PerkinElmer) for 5min at RT. Slides were mounted in Fluoromount (Invitrogen).

Whole mount TUNEL staining

Whole mount TUNEL was performed as described previously[99] using the Apoptag Peroxidase in situ Apoptosis Detection kit (Millipore) according to the manufacturer's instructions. Embryos were digested with 10 μg/mL proteinase K for 3 min, followed by 1h incubation with the terminal deoxynucleotidyl transferase at 37°C. Cell death was detected using the alkaline phosphatase-conjugated anti-digoxigenin antibody (Roche) and NBT/BCIP (Roche) as a substrate.

Image acquisition

Brightfield images were obtained using a Hamamatsu Nanozoomer 2.0 slide scanner with a 20× objective. Immunofluorescence images were acquired using a Leica SP8 confocal microscope with a 40× objective. 3D image acquisition of optically cleared samples was performed using a Zeiss Lightsheet Z1 microscope with a 20X objective. Images were analysed using ImageJ software and figures composed with Adobe Photoshop.

QUANTIFICATION AND STATISTICAL ANALYSIS

A power calculation using the SCOPIT tool v1.1.4 (https://alexdavisscs.shinyapps.io/scs_power_multinomial/), designed for scRNA-seq experiments, indicates that the 1589 cells present in the CR differentiation trajectory we describe here are sufficient to capture at

Please cite this article in press as: Moreau et al., Repurposing of the multiciliation gene regulatory network in fate specification of Cajal-Retzius neurons, Developmental Cell (2023), https://doi.org/10.1016/j.devcel.2023.05.011

least 10 cells of any state representing 1% of the total population with a 95% confidence interval. At least two biological replicates (embryos) were analysed by histology as indicated in figure legends. Quantifications of cell distribution shown in Figure 7 were done manually by counting the total number of recombined (GFP^+) cells in each region. For each embryo, at least 3 sections were cumulated. For the centriolar status, cells were manually classified as single or multiple FOP and the % of each category calculated for each section. Quantification of basal progenitors in the hem shown in Figure S4B was done manually by counting the number of $Tbr2^+$ cells.

ADDITIONAL RESOURCES

A Shiny App to visualize scRNAseq data is available at: https://apps.institutimagine.org/mouse_hem/

Developmental Cell, Volume *58*

Supplemental information

Repurposing of the multiciliation gene regulatory network in fate specification of Cajal-Retzius neurons

Matthieu X. Moreau, Yoann Saillour, Vicente Elorriaga, Benoît Bouloudi, Elodie Delberghe, Tanya Deutsch Guerrero, Amaia Ochandorena-Saa, Laura Maeso-Alonso, Margarita M. Marques, Maria C. Marin, Nathalie Spassky, Alessandra Pierani, and Frédéric Causeret

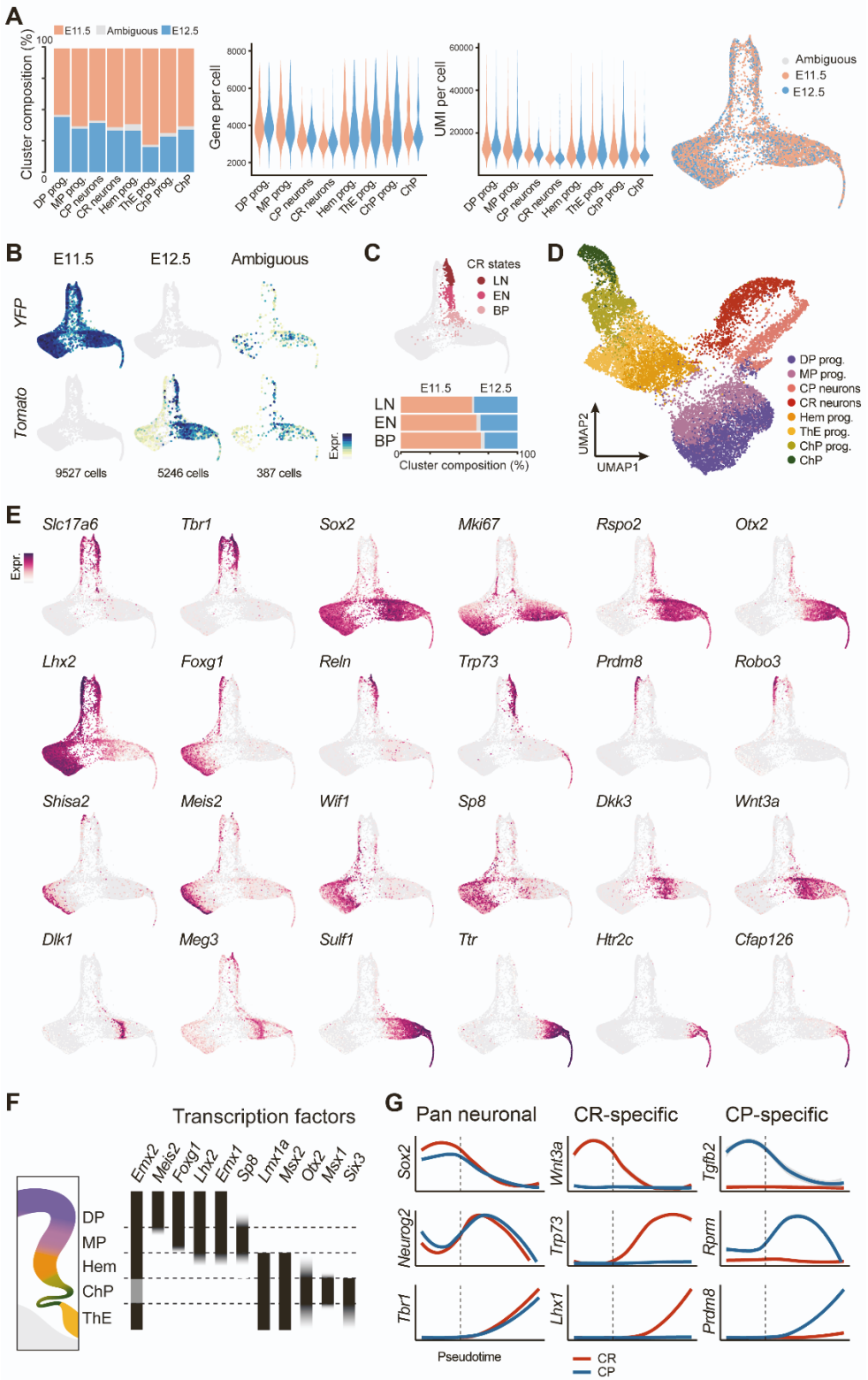

Figure S1. Additional gene expression patterns – Related to Figure 1

(A) Estimated contribution of cells collected at E11.5 or E12.5 to each cluster, comparison of the number of genes and UMI per cell at each age, and SPRING plot of the estimated collection stage. (B) Expression of *YFP* and *Tomato* transcripts split by estimated age. (C) Contribution of cells collected at E11.5 and E12.5 to CRs differentiation states (BP: basal progenitors, EN: early neurons, LN: late neurons). (D) UMAP dimensionality reduction of the dataset. (E) Expression of selected genes on the SPRING dimensionality reduction used to annotate the dataset (F) Illustration of the expression of selected transcription factors in progenitor domains (G) Smoothed expression dynamics of selected genes along CRs (red) and CP neurons (blue) differentiation. The dashed line represents the exit of apical progenitor state.

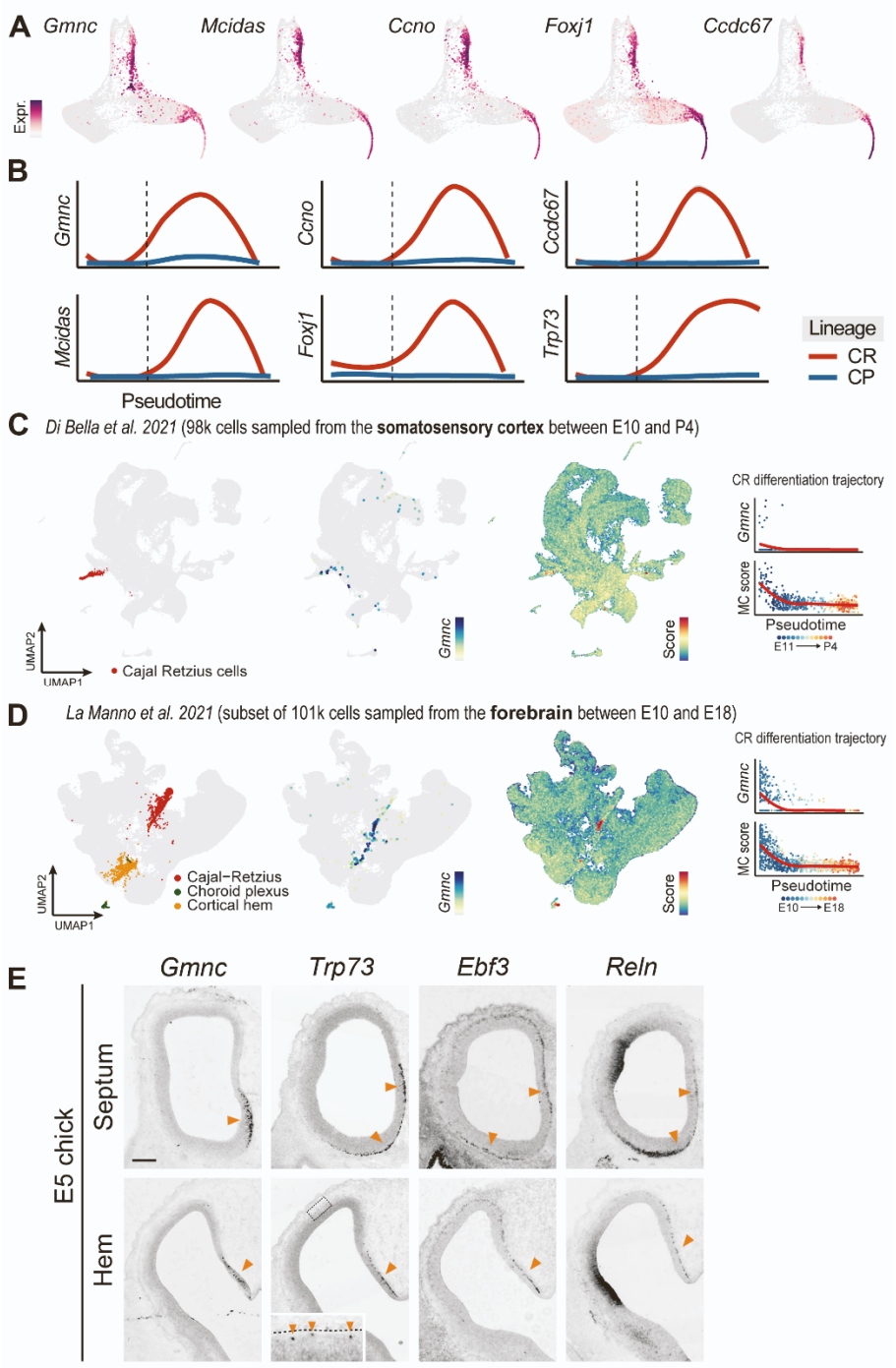

Figure S2. Expression of multiciliation genes – Related to Figure 2

(A) Expression of selected multiciliation genes on the SPRING dimensionality reduction used to annotate the dataset (B) Smoothed expression dynamics of multiciliation genes along CRs (red) and CP neurons (blue) differentiation. The dashed line represents the exit of apical progenitor state. (C) scRNAseq data from Di Bella et al. [35] illustrating the specific expression of *Gmnc* and enrichment of the multiciliation signature (same as Figure 2C) in CRs. The plots on the right correspond to the maturation trajectory of CRs and show that expression of multiciliation genes is restricted to the onset of CR differentiation. (D) same as C for a subset of the La Manno et al. [34] dataset (forebrain cells only). The increased capture of multiciliation genes expression compared to C reflects cell sampling that included regions of CR production (the hem in particular), whereas C contains CRs that migrated away from their source and invaded the somatosensory cortex. (E) ISH for *Gmnc*, *Trp73*, *Ebf3* and *Reln* on coronal sections of E5 chick embryos at the level of the septum and hem. Arrowheads point to signal in the marginal zone. The high magnification for *Trp73* illustrate the few positive cells found in the dorsal cortex, far from the hem. Scale bar: 200µm

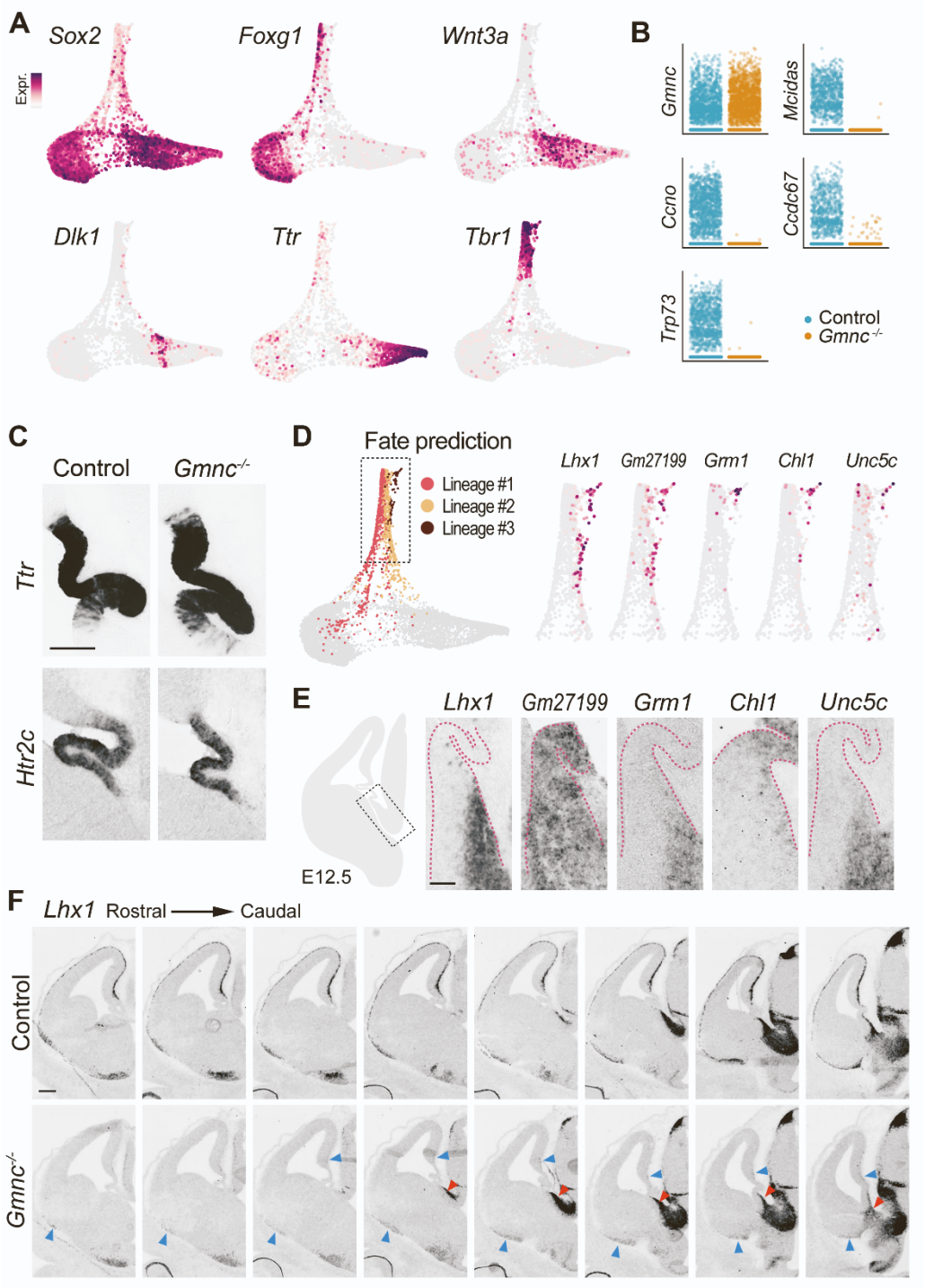

Figure S3. Additional characterization of *Gmnc* mutants – Related to Figure 4
(A) Expression of selected genes on the SPRING dimensionality reduction of the *Gmnc* mutant dataset. (B) Comparative expression of multiciliation genes in control (blue) and *Gmnc* mutant (orange) cells. Mutant *Gmnc* transcripts lack exons 3 and 4 but retain the 3'UTR and are therefore detected by scRNAseq. (C) ISH for ChP-specific genes on coronal sections of E12.5 control or mutant embryos. (D) Neuronal lineages identified in the *Gmnc* mutant dataset. High magnifications (right panel) illustrate the expression of selected markers of the small population that was excluded from subsequent analyses. (E) ISH for genes shown in (D) on coronal sections of the E12.5 ThE from wild-type embryos. (F) ISH for *Lhx1* on coronal sections of the E12.5 forebrain from wild-type and *Gmnc* mutant embryos. Red arrowheads point to the ThE, blue arrowheads indicate the rare *Lhx1*$^{+}$ cells observed in the telencephalic marginal zone of *Gmnc* mutants. Scale bars: 100µm in (C), 50µm in (E), 200µm in (F).

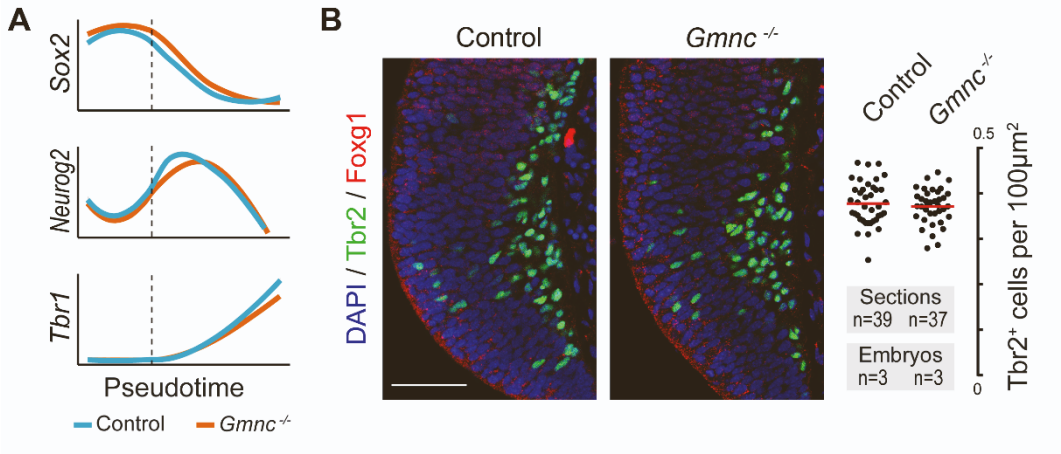

Figure S4. Neurogenesis in *Gmnc* mutants – Related to Figure 4
(A) Temporal dynamics of genes expressed in apical progenitor (*Sox2*), basal progenitors (*Neurog2*) or differentiated neurons (*Tbr1*) during CRs differentiation in control (blue) and *Gmnc* mutant (orange) datasets. The dashed lines correspond to the exit of apical progenitor state. (B) Immunostaining on coronal sections of E12.5 control or *Gmnc* mutant embryos showing basal progenitors and early neurons ($Tbr2^+$, green, rabbit antibody) in the hem region identified by the absence of Foxg1 (red) staining. Quantification of the density of $Tbr2^+$ cells revealed no significant differences between control and mutants. Scale bar: 50µm.

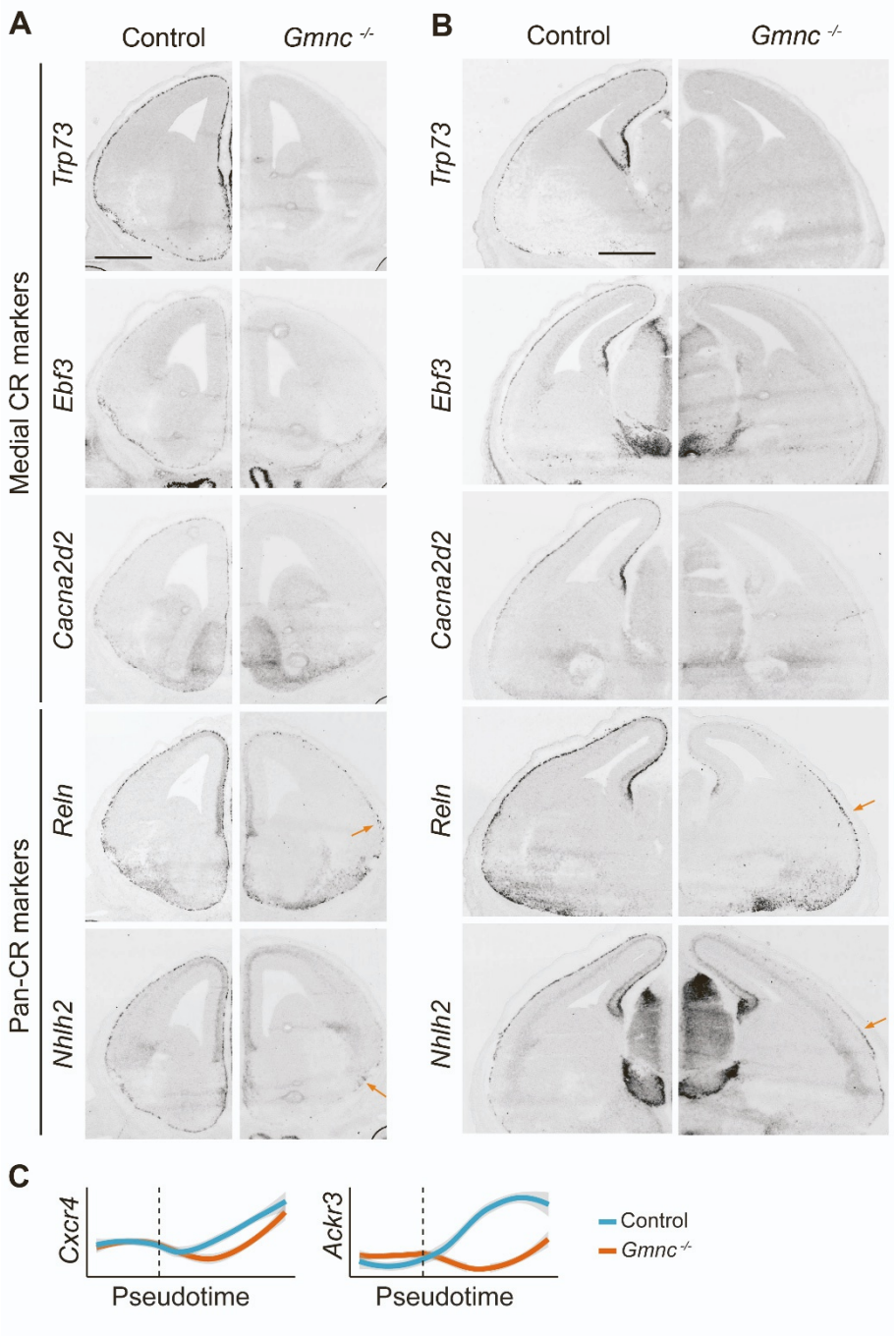

Figure S5. Expression of CR marker genes in *Gmnc* mutants – Related to Figure 5
(A) ISH for marker genes of medial CRs (*Trp73*, *Ebf3*, *Cacna2d2*) or all CRs subtypes (*Reln*, *Nhlh2*) on coronal section at rostral levels of E13.5 *Gmnc* mutants and controls. (B) same as A at caudal levels. Arrows point to remaining CRs in lateral and ventral regions of mutants. (C) Temporal dynamics of *Cxcr4* and *Ackr3/Cxcr7* expression during CR differentiation in control (blue) and *Gmnc* mutant (orange) datasets. The dashed lines correspond to the exit of apical progenitor state. Scale bars: 500µm.

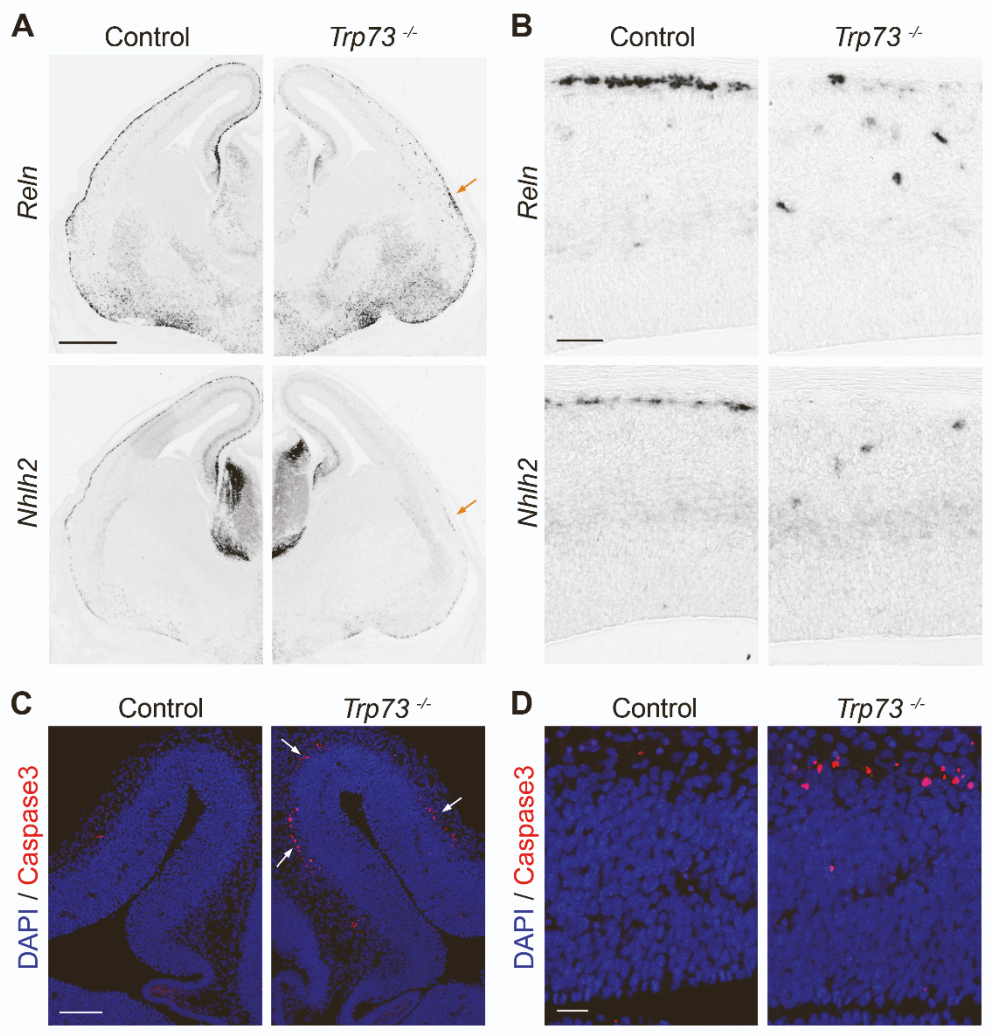

Figure S6. Phenotype of *Trp73* mutants – Related to Figure 6
(A) ISH for *Reln* and *Nhlh2* on coronal section of E13.5 *Trp73* mutants and controls. Arrows point to the few remaining CRs in lateral and ventral regions. (B) High magnification of the dorsal cortex showing the few ectopic CRs found deep into the cortical plate in mutants instead of their normal superficial position. (C) Immunostaining against activated Caspase-3 (red) on coronal section of E13.5 *Trp73* mutants and controls showing increased apoptosis (arrows) in the marginal zone of *Trp73* mutants. (D) High magnification of the images shown in (C). Scale bars: 500µm in (A), 50µm in (B), 100µ in (C), 20µ in (D).

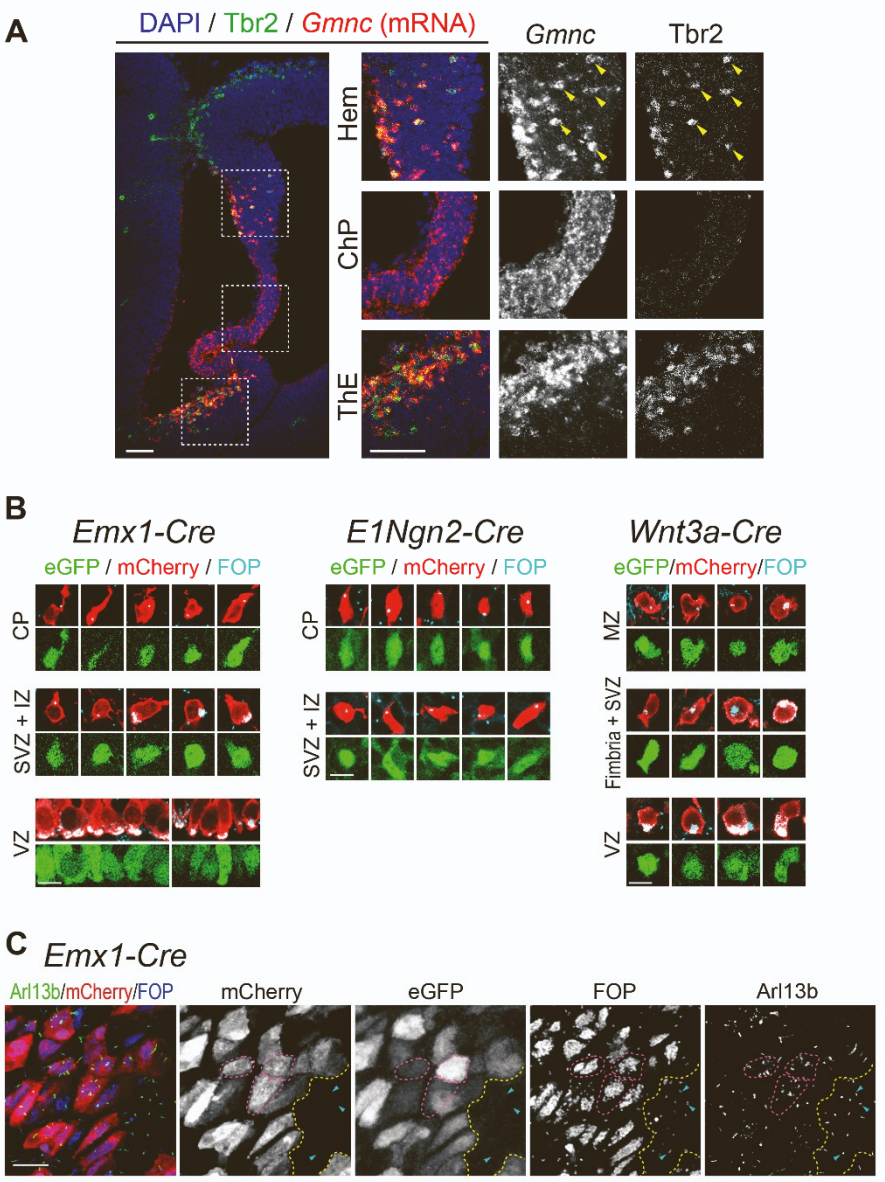

Figure S7. Centriolar amplification upon *Gmnc* electroporation – Related to Figure 7
(A) Combined in situ hybridisation for *Gmnc* (red) and immunostaining for Tbr2 (green, rat antibody) on coronal sections of an E12.5 embryo showing high correlation in the hem and ThE. (B) Immunostaining for centrioles (FOP, Cyan) on representative electroporated (mCherry^{+}, red) and *Gmnc*-expressing cells (eGFP^{+}, green) used to draw cell shapes shown in Figure 7D-F. (C) *En face* whole mount of an *Emx1*^{Cre} electroporated brain immunostained for cilia (Arl13b) and centrioles (FOP) showing a region containing electroporated (mCherry^{+}) and *Gmnc*-expressing (eGFP^{+}) cells. Targeted cells often display multiple cilia (as exemplified with pink dashed lines) whereas the untargeted region (between yellow dashed lines) typically contains single FOP/Arl13b foci (blue arrows). Scale bars: 50µm in (A), 10µm in (B) and (C). VZ: ventricular zone, SVZ: subventricular zone, IZ: intermediate zone, CP: cortical plate, MZ : marginal zone.